2020

Nanofiber Scaffolds as 3D Culture Platforms

Stephanie Bule
Michigan Technological University, sebule@mtu.edu

NANOFIBER SCAFFOLDS AS 3D CULTURE PLATFORMS

By

Stephanie E. Bule

A THESIS

Submitted in partial fulfillment of the requirements for the degree of

MASTER OF SCIENCE

In Biomedical Engineering

MICHIGAN TECHNOLOGICAL UNIVERSITY

2020

This thesis has been approved in partial fulfillment of the requirements for the Degree of MASTER OF SCIENCE in Biomedical Engineering.

Department of Biomedical Engineering

Thesis Advisor: *Dr. Smitha Rao*

Committee Member: *Dr. Jeremy Goldman*

Committee Member: *Dr. Marina Tanasova*

Department Chair: *Dr. Sean Kirkpatrick*

Table of Contents

List of figures

Preface

The scaffolds used for the experiments were fabricated by Samerender Nagam Hanumantharao and Carolynn Que from the Biomedical Microdevices lab in the Biomedical Engineering Department at Michigan Technological University. Intensity analysis of quantitative images and immunostaining was done in collaboration with Samerender Nagam Hanumantharao.

The fluorescent probes 1-amino-2,5-anhydro-d-mannitol with an H group attached at the c4 position of the coumarin ring (ManCou-H) were provided by Dr. Tanasova's lab in the Chemistry Department at Michigan Technological University.

Acknowledgements

I would like to first and foremost thank my advisor, Dr. Rao for her continual guidance, advice and support as my mentor. I appreciate your encouragement to pursue areas that previously challenged me, to go beyond what I thought was not possible and to achieve my graduate student goals. I'd also like to thank the members in the Biomedical Microdevices lab at Michigan Technological University. Samerender, Carolynn, Srinivas and Brennan, it has been a pleasure to work beside you as fellow students and colleagues. You have all contributed to making the lab a great environment to conduct research. I'm very thankful for all the help you've extended to me in these experiments while pursuing projects of your own.

I'd also like to thank my friend Bernadette for being a constant pillar of support here in Houghton. I'm very appreciative to have someone that encourages me to become the very best version of myself as a person, a student, and a friend.

Words cannot express how grateful I am to have the family that I do. Thanks to my mom and dad for having a continuous faith in my capabilities in pursuing a graduate career. Thank you for your love and your unwavering dedication to support our family in all that we set our minds to. Your example of hard work and perseverance throughout the years have carried me through the hardest of times while away at school. To my siblings, nieces and nephew, thank you so much for the constant encouragement and support. I would not be where I am if it was not for you all.

Finally, I would like to thank God for His continual protection, guidance and provision while away at school. I'm grateful for the strength and support to help bring this dream of mine to fruition. This could not have happened without Your constant grace.

Abstract

Cell culture has become the basis for understanding the fundamental mechanisms of cell, tissue and organ function. Although major advancements in uncovering the underlying processes and mechanisms of normal and diseased cell biology have been made by using two-dimensional (2D) cell culture, there is a recent shift in moving towards three-dimensional (3D) culture platforms. The motivation is to better recapitulate the microenvironment of cells in vivo to obtain results that are more indicative to actual cellular processes. In this study, electrospun nano-fibrous scaffolds made of polycaprolactone were used as a 3D culture tool to investigate difference in cell behavior and gene expression in normal breast epithelial cells, 184B5, and breast cancer cells MCF7 and MDA-MB-231. Cells were seeded individually as well as in cocultures on the various platforms and treated with the fluorescent fructose mimic, ManCou-H for 24h and 48h. Differences in cell behavior as well as gene expression was observed amongst the different culture platforms indicating that there are discrepancies when limiting cell culture studies to 2D platforms. The varying gene expression of both GLUT5 and cytokeratin-18 amongst the platforms indicated that 3D culture platforms should be considered in experiment design.

1 Introduction

1.1 Extracellular Matrix

One of the major known functions of the extracellular matrix (ECM) is that it provides structural support for organs, tissues, and individual cells [1]. More attention has recently been given to the mechanical characteristics of the ECM and how the stiffness and deformability play a role in cell behavior [2]. Cells are able to sense their microenvironment through the numerous transmembrane proteins, and the through their interactions between with the surrounding matrix which in turn leads to a cascade of cell signaling events through the receptors and different cell receptors that can trigger various cellular responses [3]. The ECM is involved in different physiological processes of cells including differentiation, proliferation, migration, morphology and gene expression [2]. Recently, studies show that the ECM is also responsible for the onset of a number of several diseases such as the progression of neoplastic disease as well as the mechanical properties of the ECM affecting the motility of various carcinoma cells [4] [5].

ECM stiffening has been shown to initiate epithelial to mesenchymal transition (EMT), whereby cells that are held together by tight junctions lose their epithelial cell like properties and gain mesenchymal cell like characteristics [6]. In breast cancer, EMT has shown to play a significant role in tumor progression and metastasis [7]. The EMT process is further characterized by the loss of cell to cell adhesion molecules such as E-cadherin and cytokeratin as well as the gaining mesenchymal cell associated proteins such as N-cadherin, vimentin and fibronectin [6]. Research shows that distant metastases for epithelial cancers such as breast cancer can be attributed to this EMT process [8]. The transition between losing epithelial characteristics and gaining mesenchymal morphology causes an increase in cell motility and their ability to create metastatic subpopulations at various distant sites in the body [9].

Cytokeratin's are crucial in the structural integrity of cells by forming cytoplasmic networks of intermediate filaments [10]. Cytokeratin 18 (CK18) is present in single-layered epithelial tissues and has been shown to provide an intracellular scaffold which can resist any stresses that have been externally applied to the cell [11]. More importantly, CK18 is recognized as an epithelial biomarker and has been shown to vary in tumor cell behavior [12]. It has been reported that non-metastatic breast cancer cell lines exhibit a high CK18 expression verses metastatic breast cancer cell lines exhibit a low CK18 expression [13]. Therefore, the upregulation or downregulation of CK18 can be used to provide insight in tumor progression.

1.2 Cell Culture methods and limitations

Given that the cell microenvironment is strongly affected by the mechanical and biochemical stimuli from the ECM, it should be considered when studying cellular behavior *in vitro*. Two-dimensional (2D) systems have advanced scientific understanding

of cell behavior and are a widely accepted model for *in vitro* studies. A present challenge when studying cellular processes and disease progression in 2D models is that these culture methods fail to recapitulate the structural components that are exhibited in vivo. Emerging evidence shows that there are differences in cell to substrate interactions as well as in cellular adhesion and migration [14]. This provides an explanation as to why exciting potential new therapies that provide positive results *in vitro* fail to provide the same efficacy in preclinical and clinical studies. Animal models remain the primary source for preclinical studies, however they still pose a challenge as they do not allow for the direct investigation disease progression or the specific microenvironmental cues that are associated with it [15]. More so, the rate of successful translation between animal testing and clinical trials has been shown to be less than 8% given that animal models cannot mimic the complex processes exhibited by human carcinogenesis and tumor progression.

Other 3D models that have been used in cell culture that will be discussed include spheroids and hydrogels. Spheroid models have been widely accepted as 3D culture models over the past couple of decades. One of the most common ways to produce spheroids is via the hanging drop technique whereby cell droplets hang on the lid of a tissue culture dish through the surface tension [16]. Gravity then will induce an aggregate formation of cells into a single cluster forming a spheroid. Multicellular spheroids are also possible and can mimic living tissues observed *in vivo* in regards to their bio-functional as well as biophysical characteristics [17]. However, using spheroid models still pose certain challenges as it is not suitable for long term culture, it can be time consuming, tedious and unstable [18].

Hydrogels, which rely primarily on crosslinked networks that contain high water content have been widely used as scaffolds as 3D models [19]. Previous studies have shown the efficacy of engineered 3D hydrogels in promoting cell viability, adhesion, differentiation, proliferation and migration by controlling the presence of specific mechanical and biochemical cues [20-23]. Recently biodegradable polymers have been used to enhance these models by gradually degrading to allow for matrix production and continued cellularization [24]. One hurdle in using hydrogels as 3D culture models is that is it difficult to match hydrogel degradation to the rate of tissue formation which is very important in retaining the three-dimensional shape as well as the mechanical integrity of the resulting culture model [25].

1.3 Scaffolds

Biocompatible three-dimensional (3D) scaffolds have emerged as a contender in 3D cell culture in order to simulate conditions similar to the extracellular matrix [26]. Ideally, these synthetic scaffolds should mimic an environment that is a suitable substitute for the natural ECM in order to provide the essential biophysical and topographical cues (cell to matrix, and cell to cell interactions) that are absent in 2D culture methods. Nanofibrous scaffolds are very similar in morphology and dimensionality to the fibrillar structure that is shown by the ECM as they allow cells to migrate into the scaffold and proliferate through the porous nanofibers [27]. Specifically, electrospun polycaprolactone

(PCL) scaffolds have been shown to provide a suitable growth environment for breast normal as well as breast cancer cells [28]. The simple process of electrospinning allows for the fine tuning of the mechanical and physical properties of these scaffolds by using the electric field to control the formation of the crystalline bonds in PCL. This is done by manipulating both the flow rate and the electric field during scaffold fabrication [29]. One major advantage in using these nanofibrous scaffolds is that the level of control over the nano-features that allows for batch to batch reliability as well as consistency in topographical features and mechanical properties. The consistency provided by the electrospinning process can allow for increased integrity of cell culture in that many experiments can be done on scaffolds of identical topography and morphology.

1.4 Breast Cancer and GLUT 5

As mentioned previously the ECM plays a role in the onset of neoplastic diseases, one of such being breast cancer. Cancer cells rapidly proliferate, and as a result, have metabolic abnormalities to allow them to adapt to such vigorous growth [30]. Contrary to normal cell function, instead of completing glycolysis and entering oxidative phosphorylation, cancer cells will continuously perform glycolysis generating a large amount of lactic acid even when oxygen is present [31]. This phenomenon is known as the Warburg effect, and it explains how cancer cells will consume high amounts of glucose leaving their microenvironment depleted of nutrients. This lack of glucose will cause cancer cells to look for other nutrient sources as substitutes to continue their rapid cell growth [32].

Cancer cells are known to overexpress a family of hexose transporters classified as GLUTs in order to keep up with the high energy demand in their growth and proliferation [33]. GLUT1, the main transporter for D-glucose is overexpressed in cancer cells that have mutants of the tumor suppressor protein, p53 and as such, it has shown that the normal p53 protein inhibits GLUT1 expression [34]. In contrast to other cancers, it has been previously shown that 42% of breast tumors express lower levels of GLUT1 and express higher levels of D-fructose transporters GLUT5 and GLUT2 instead [35]. Excessive fructose consumption was reported to be correlated to tumorigenesis and tumor progression [36-38]. Given the report that states that normal breast cells do not overexpress GLUT5, it has been suggested that GLUT5 expression could be used as a tool to selectively target breast tumors in breast cancer diagnostics [39].

Many fructose-based derivatives have been studied as imaging tools for distinguishing cancer populations from non-cancer populations. Fluorescently labeled fructose conjugates such as 7-nitrobenzofurazan (NBDF) have been used to specifically target fructose transporters [40]. Other studies have shown that fluorescently labeled 1-amino-2,5-andhydro-D-mannitol have a higher affinity to fructose specific transporters than actual fructose [41]. Furthermore, GLUT5 reporters that have been extended with coumarin conjugates of 1-amino-2,5-deoxy-D-mannitol show high affinity and specificity towards GLUT5 provide a range of fluorescent fructose mimics that can be used as tools for breast cancer detection [41, 42].

1.5 My Approach

The present studies aim to compare electrospun PCL scaffolds systems as 3D cell culture tools against traditional 2D cell culture plates. PCL scaffolds were selected due their ability to mimic the ECM structure in mechanical and physical properties. Breast normal as well as breast cancer cell lines were seeded in single culture as well cocultures and were subjected to normal culture conditions as well as conditions containing fluorescently labeled fructose mimics. After 24 and 48 hours, samples were imaged and the presence of GLUT5 and cytokeratin-18 was analyzed. The results show variability in GLUT5 and cytokeratin-18 across different types as well as the culture plate. Cell behavior of cocultures appears to be more aggregate and clustered on 2D culture plates and more spread out on 3D scaffold systems.

2 Materials and Methods

2.1 Cell lines and cell culture

Human breast epithelial normal cells (184B5/ ATCC® CRL-8799™), adenocarcinoma (MCF-7/ATCC® HTB-22™) cells and triple negative breast cancer (MDA-MB-231/ATCC® HTB-26™) were procured from American Type Cell Culture. 184B5 cells were cultured in MEBM base medium from Lonza/Clonetics Corporation supplemented with MEGM (CC-3150) supplement kit along with penicillin-streptomycin (Life Technologies, USA) to a final concentration of 1%. The gentamicin supplement from the kit was not used as recommended by ATCC and cholera toxin was not added. MCF7 and MDA-MB-231 cells were cultured in RPMI 1640 [+] L-glutamine from Corning which was supplemented with fetal bovine serum, FBS (Life Technologies, USA) to a final concentration of 10% along with penicillin-streptomycin (Life Technologies, USA) to a final concentration of 1%. Cells in exponential growth phase were treated with trypsin, counted using a hemocytometer, seeded and incubated and maintained under standard cell culture conditions (37 °C, 65% relative humidity, 5% CO_2). Culture media was changed every 2 alternate days.

2.2 Scaffold Sterilization

Electrospun polycaprolactone (PCL) scaffolds of aligned, honeycomb and random topographies were obtained from the Biomedical Microdevices lab from Michigan Technological University. Scaffolds were cut into approximately 1x0.5 cm^2 area, sterilized in 70% ethanol, irradiated with UV radiation for one hour and allowed to dry in a sterile biosafety cabinet. Scaffolds were then placed into supplemented RPMI culture media for 24 hours prior to cell seeding.

2.3 Fructose mimic probe preparation

2,5-anhydro-D-mannitol-coumarin based GLUT5-specific probe (ManCou-H) was obtained from the Chemistry department at Michigan Technological University. Probes were received at a concentration of 5mM and were diluted to a final working concentration of 20μM. This concentration was chosen based off previous studies showing that 20μM of ManCou-H probe is sufficient for visualizing probe uptake [42]. Probes were diluted in supplemented RPMI 1640 culture media, protected from light.

2.4 Live cell tracking

Cell Tracker Red CMTPX (Life Technologies, USA) was made at a concentration of 5μM using serum free RPMI culture media. Cell Tracker Green CMFDA (Invitrogen™) was made at a concentration of 5μM using serum free RPMI culture media as well as supplemented MEGM culture media. Culture media was removed from culture plates

containing cells and 5mL of the cell tracker red solution was added to MCF7 and MDA-MB-231, and cell tracker green solution was added to 184B5 and MDA-MB-231 using solutions containing their respective culture media. The cells were incubated for 45minutes at 37°C, protected from light in the incubator. The culture media on scaffolds was removed prior to cell seeding. Cells were then treated with trypsin, cell counted using a hemocytometer and seeded onto the scaffolds at a density of 3,000 cells per scaffold, placed in non-treated 24 well culture plates (Celltreat™) and incubated at 37°C for 30 minutes to allow for cell attachment to scaffolds. Cells were also seeded at a density of 3,000 cells per well onto 96 well treated culture plates. Supplemented RPMI 1640 media with and without ManCou-H probe was then added to scaffolds and culture plates and cells were incubated at 37°C. Cells were visualized via fluorescence microscopy (EVOS FL Auto) after 24h and 48h of growth. The excitation and emission for the cell tracker red was 577nm/602nm, the excitation and emission for the cell tracker green was 492nm/517nm, finally the excitation and emission for the ManCou-H probe was 366nm/452nm. The quantitative analysis of the cell behavior was done using ImageJ software (NIH).

2.5 Culture preparation for immunocytochemistry

The culture media on scaffolds was removed prior to cell seeding. Cells were then treated with trypsin, cell counted using a hemocytometer and seeded onto the scaffolds at a density of 3,000 cells per scaffold, placed in non-treated culture plates and incubated at 37°C for 30 minutes to allow for cell attachment to scaffolds. Cells were also seeded at a density of 3,000 cells per well onto treated culture plates. Supplemented RPMI 1640 media with and without ManCou-H probe was then added to scaffolds and culture plates and cells were incubated at 37°C. Cells were visualized via fluorescence microscopy (EVOS FL Auto) after 24h and 48h of growth.

2.6 Immunocytochemistry

In this section, both culture plates and scaffolds that were used in the experimental process both be referred to as “samples”. Samples were fixed using 4% paraformaldehyde (Electron Microscopy Sciences) diluted with 1x PBS solution, incubated at 4°C for 20 minutes. PFA was removed and the samples were rinsed with 2mL of PBS twice for 15 minutes. Blocking solution was made using Triton X-100 (ACROS Organics™), bovine serum albumin (Fischer Scientific), and donor horse serum (Corning Media Tech). 300µL of blocking solution was added to the samples and incubated overnight at room temperature (RT). Blocking solution was removed and primary antibody (A86656 abcam/1:500 dilution) was added to the samples and incubated at RT for approximately 2 hours. Primary monoclonal anti-mouse antibody (MA 1-036X, Thermo Fischer Scientific/ 1:500 dilution) incubation buffer was removed and samples were rinsed with PBS twice for 15 minutes. Secondary goat anti-mouse antibody solutions of AlexaFluor Plus 488 GLUT5 (Santa Cruz Biotechnology /1:400 dilution) and AlexaFluor 488 Cytokeratin 18 (Invitrogen/1:500 dilution) were added to the respective samples and incubated at RT for 60 minutes. Secondary antibody incubation buffer was removed, and samples were rinsed with PBS

twice for 15 minutes. Samples stained with cytokeratin 18 were also stained with NucRed Live 647 (Invitrogen) according to manufacturer's protocols. Samples were stored at 4°C in PBS solution, protected from light. Antibody stains were visualized via fluorescence microscopy (EVOS FL Auto). The excitation and emission used for GLUT5 and cytokeratin-18 was 490nm/525nm.

2.7 Cell Intensity Measurements

Samples were imaged using the EVOS Fl auto imaging system with constant exposure, light, and gain settings. Images were analyzed using ImageJ software (NIH). From grayscale images, the corrected total cell fluorescence (CTCF) was calculated. Samples taken from the image were compared to the average fluorescence of the background of the same image so that the fluorescence signal from the selected region of interest was obtained. This process was repeated a total of five times for each image captured. An average fluorescence was obtained for each condition.

2.8 Flow cytometry analysis

Cell culture of all 3 cell lines were maintained as previously described and incubated in cell tracker solution as previously mentioned. Cells were treated with trypsin and spun down for 3 minutes at 1500rpm. The pellets were rinsed with PBS and cells were resuspended in either supplemented RPMI 1640 culture media, or 20μM ManCou-H probe containing media and incubated at 37°C for either 30 minutes or 1hr. Cells were then centrifuged for 3 minutes at 1500 rpm and resuspended in serum free RPMI 1640 culture media. Cells were identified and ManCou-H uptake was analyzed using flow cytometry (Attune NxT Flow Cytometer, Thermo Fisher Scientific).

2.9 Statistical analysis

Error bars in graphical data represent mean ± standard error of mean. Experiments were performed in triplicates, using 3 scaffolds per treatment group using 2D culture plate as the control. The Wilcoxon non-parametric test was used to analyze statistical differences between 24h and 48h for each condition. Error bars in graphical data represent mean ± standard error of mean. Experiments were performed in triplicates, using 3 scaffolds per treatment group using 2D culture plate as the control.

3 Results

3.1 Cell-Cell Behavior and Cell-to-Matrix Behavior Analysis

In order to analyze the differences in cell to cell behavior as well as cell to matrix behavior, cells were incubated in either cell tracker red or green and seeded on 2D culture plates and on the three different scaffold types (aligned, honeycomb, and mesh). Single cell lines of 184B5, MCF7, and MDA-MB-231 were seeded at 3,000cells and were put in either supplemented RPMI 1640 culture media or ManCou-H probe containing media for 24h and 48h. Cocultures were also seeded at a density of 1,500 cells per cell line (3,000 cells total) of cocultures containing 184B5+MCF7, 184B5+MDA-MB-231, and MCF7+MDA-MB-231. Images were taken at 10x magnification in the phase, GFP, TxRed, and DAPI channels, and were enhanced individually using ImageJ to visualize cell behavior. Cells that were cultured in supplemented without ManCou-H were not imaged using the DAPI channel.

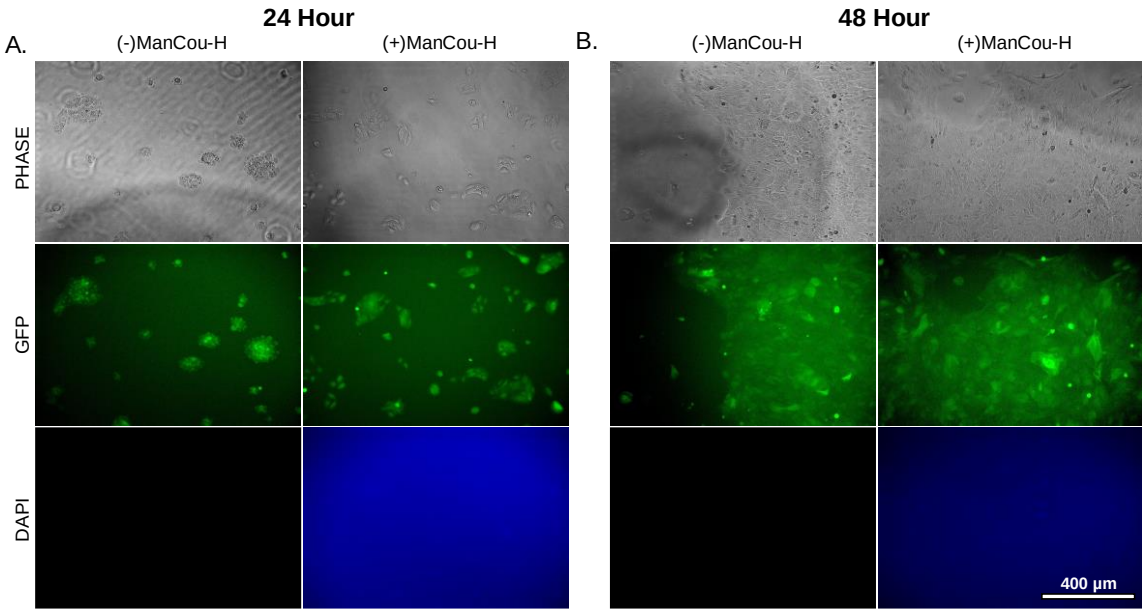

Figure 1 184B5 cells in cell tracker green seeded on 2D culture plate imaged in Phase, GFP and DAPI (A) 24 hours with and without 20µM ManCou-H media (B) 48 hours with and without 20µM ManCou-H media. Images captured at 10x magnification. DAPI images in conditions without ManCou-H were not taken.

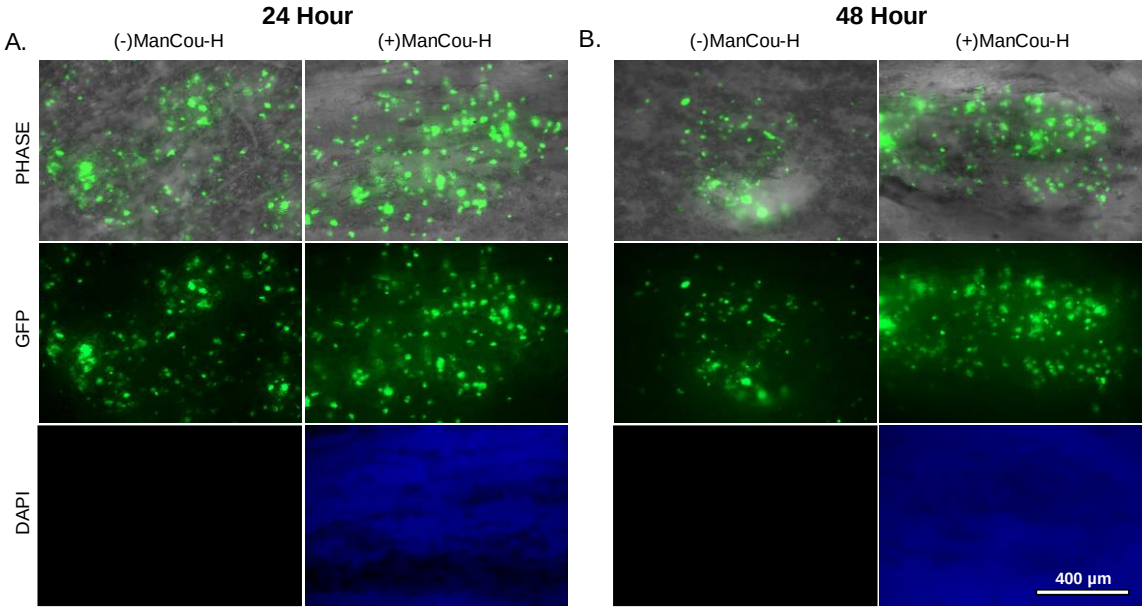

Figure 2 184B5 cells in cell tracker green seeded on aligned scaffolds and imaged in phase, GFP, and DAPI. (A) 24 hours with and without 20µM ManCou-H media (B) 48 hours with and without 20µM ManCou-H media. Images captured at 10x magnification. DAPI images in conditions without ManCou-H were not taken.

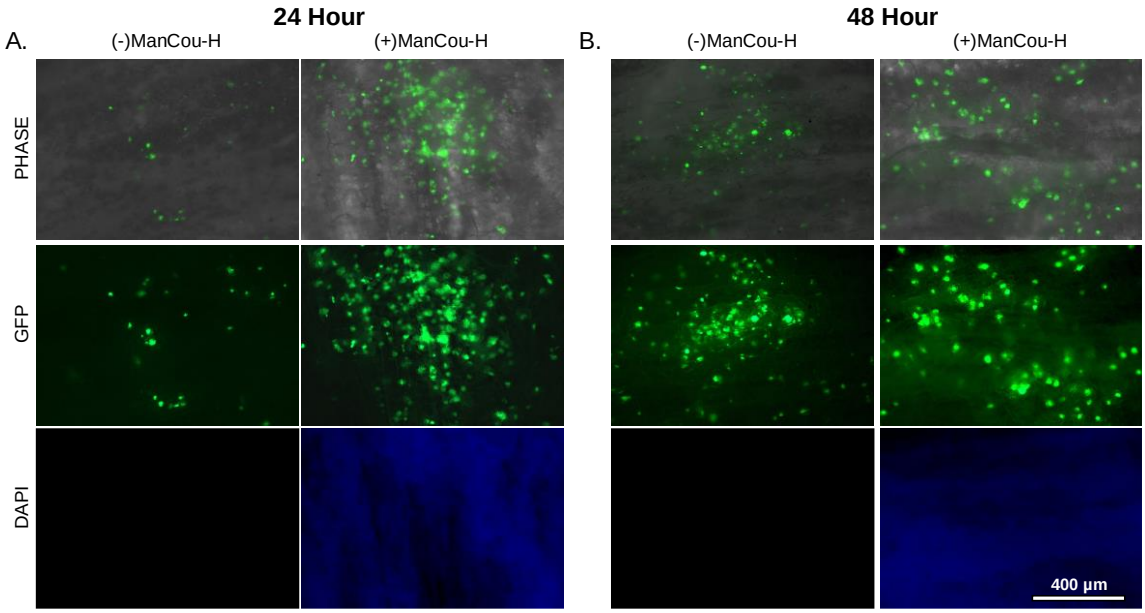

Figure 3. 184B5 cells in cell tracker green seeded on honeycomb scaffolds and imaged in phase, GFP, and DAPI. (A) 24 hours with and without 20μM ManCou-H media (B) 48 hours with and without 20μM ManCou-H media. Images captured at 10x magnification. DAPI images in conditions without ManCou-H were not taken.

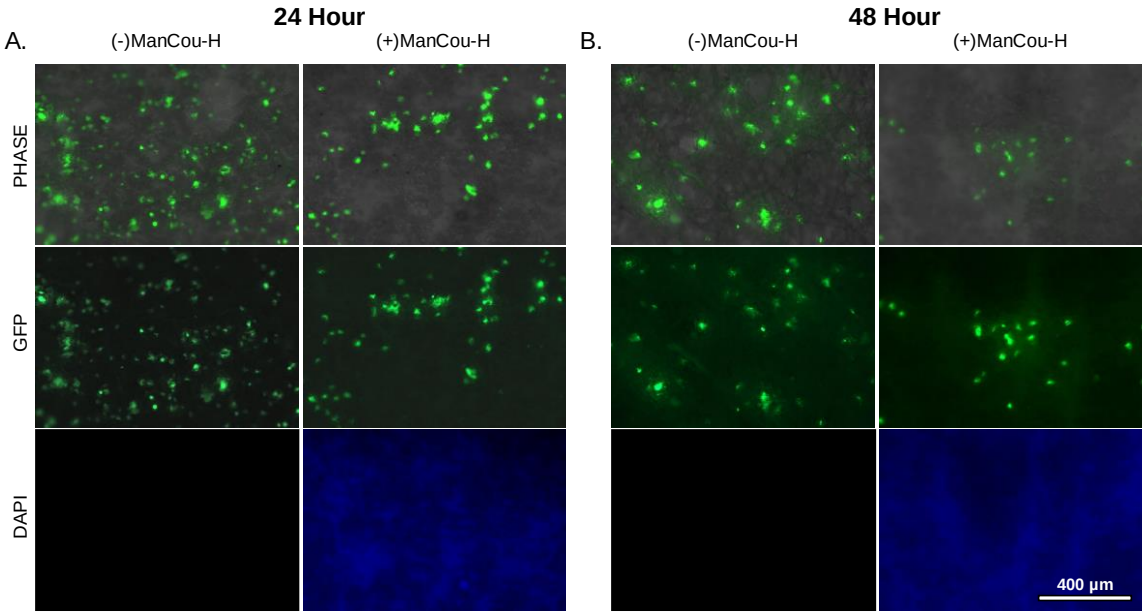

Figure 4 184B5 cells in cell tracker green seeded on mesh scaffolds and imaged in phase, GFP, and DAPI. (A) 24 hours with and without 20μM ManCou-H media (B) 48 hours with and without 20μM ManCou-H media. Images captured at 10x magnification. DAPI images in conditions without ManCou-H were not taken.

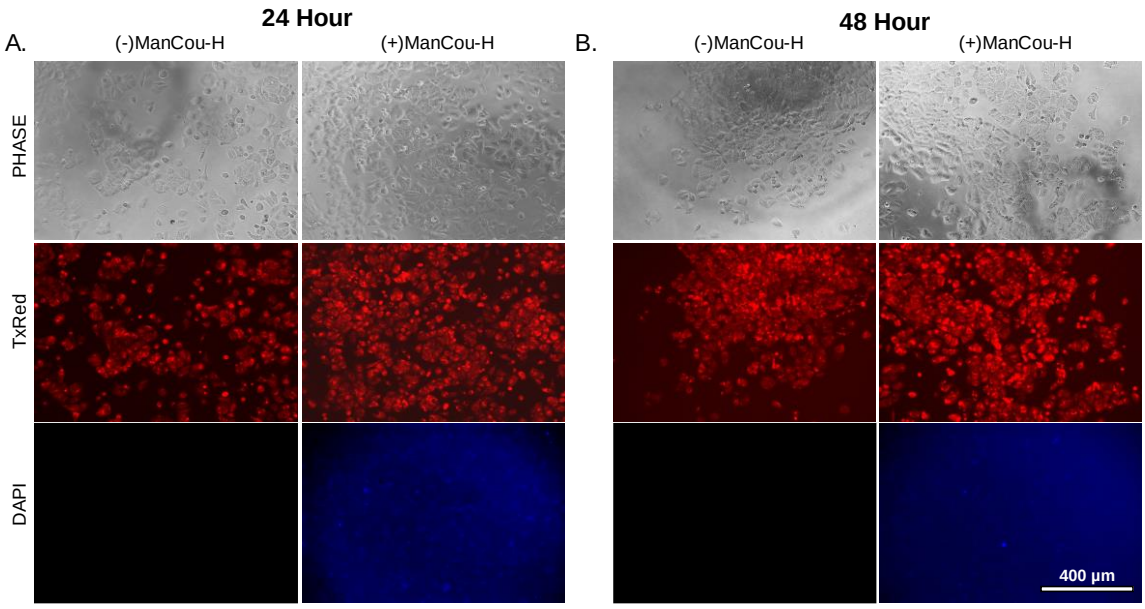

Figure 5 MCF7 cells in cell tracker red seeded on 2D culture plate imaged in Phase, TxRed and DAPI (A) 24 hours with and without 20µM ManCou-H media (B) 48 hours with and without 20µM ManCou-H media. Images captured at 10x magnification. DAPI images in conditions without ManCou-H were not taken.

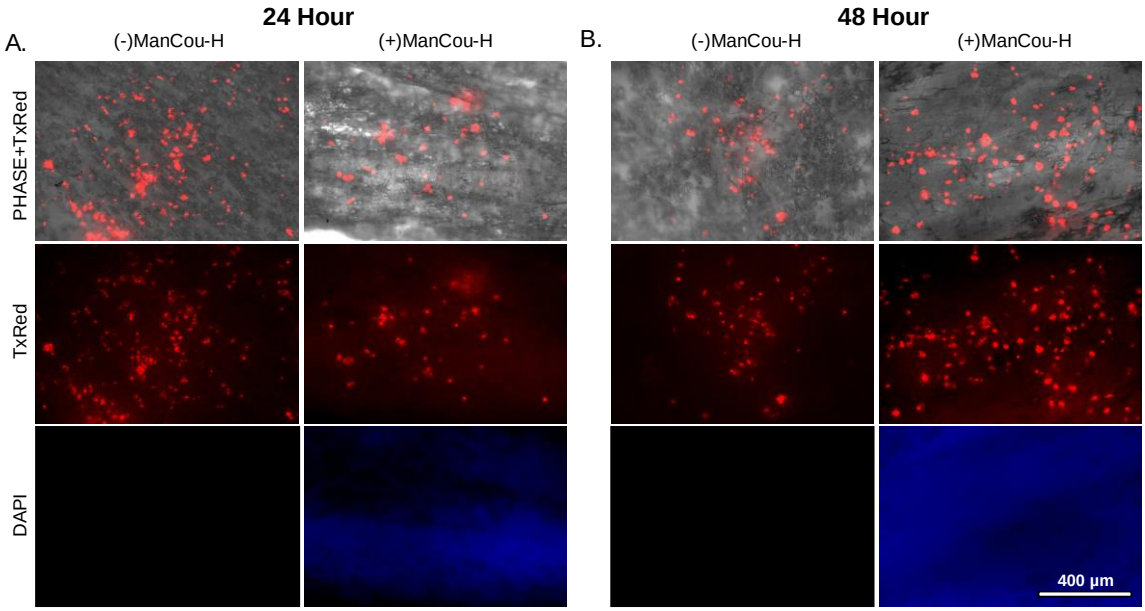

Figure 6 MCF7 cells in cell tracker red seeded on aligned scaffolds and imaged in phase, TxRed, and DAPI.(A) 24 hours with and without 20μM ManCou-H media (B) 48 hours with and without 20μM ManCou-H media. Images captured at 10x magnification. DAPI images in conditions without ManCou-H were not taken.

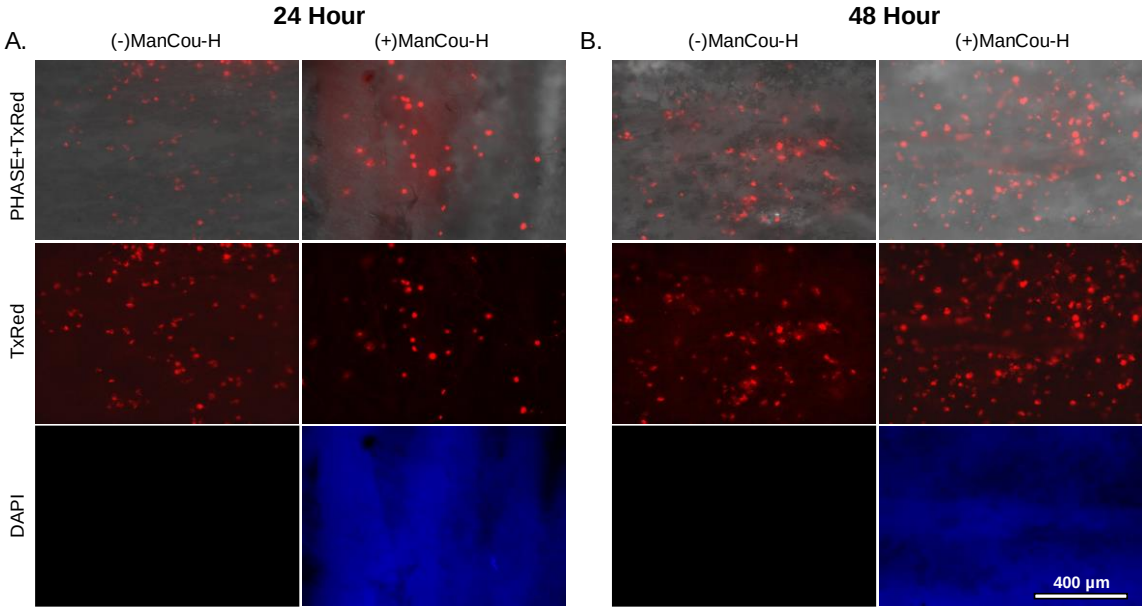

Figure 7 MCF7 cells in cell tracker red seeded on honeycomb scaffolds and imaged in phase, TxRed, and DAPI. (A) 24 hours with and without 20μM ManCou-H media (B) 48 hours with and without 20μM ManCou-H media. Images captured at 10x magnification. DAPI images in conditions without ManCou-H were not taken.

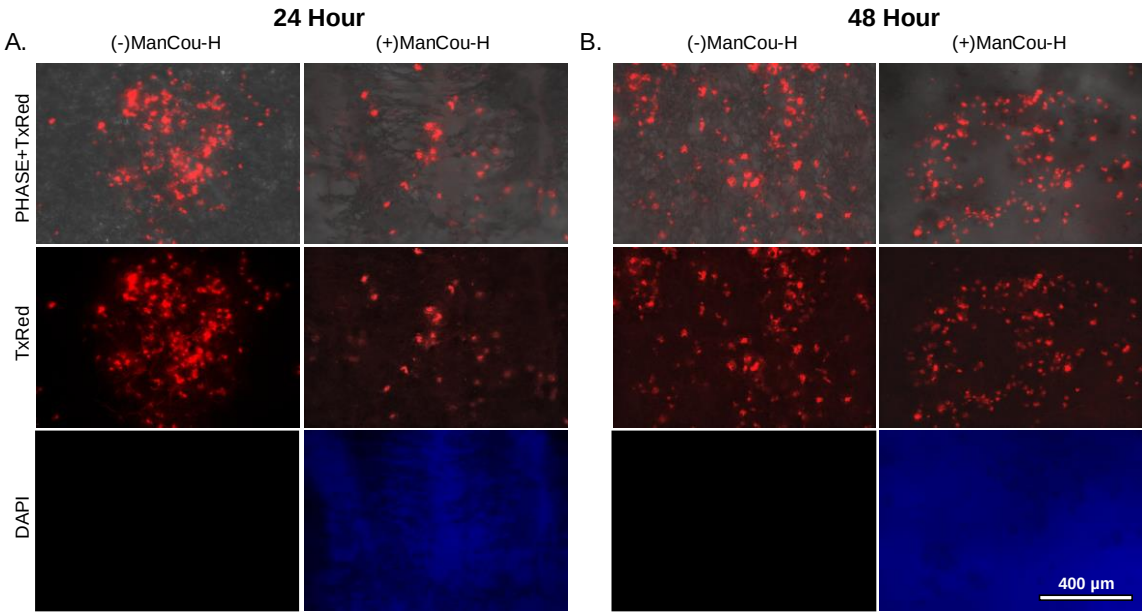

Figure 8 MCF7 cells in cell tracker red seeded on mesh scaffolds and imaged in phase, TxRed, and DAPI. (A) 24 hours with and without 20µM ManCou-H media (B) 48 hours with and without 20µM ManCou-H media. Images captured at 10x magnification. DAPI images in conditions without ManCou-H were not taken.

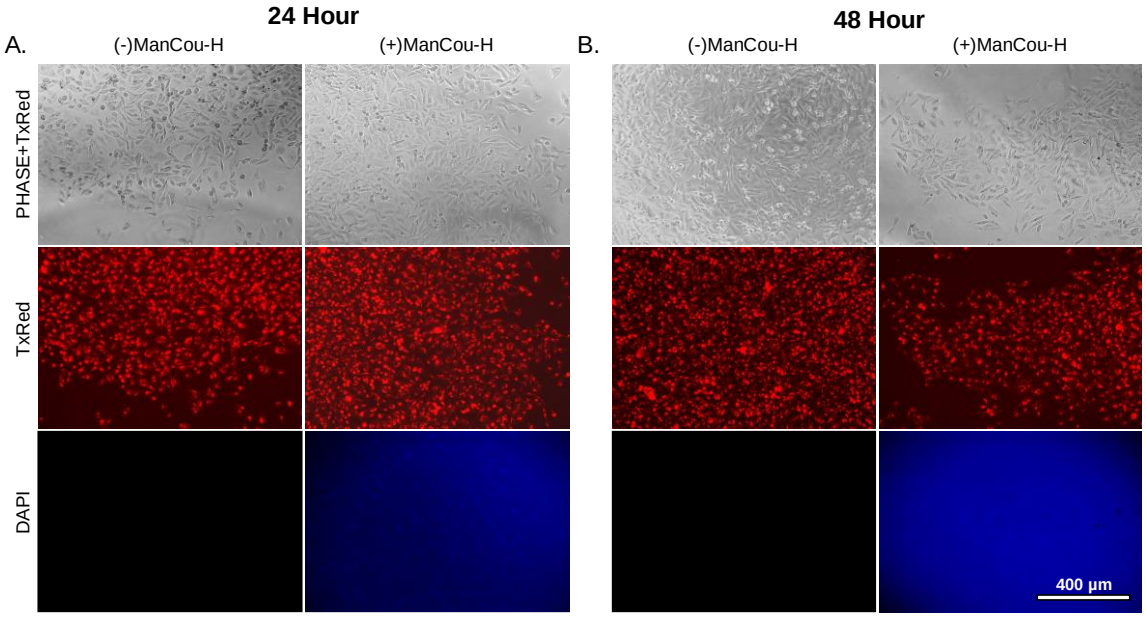

Figure 9 MDA-MB-231 cells in cell tracker red seeded on 2D culture plate imaged in Phase, TxRed and DAPI (A) 24 hours with and without 20μM ManCou-H media (B) 48 hours with and without 20μM ManCou-H media. Images captured at 10x magnification. DAPI images in conditions without ManCou-H were not taken.

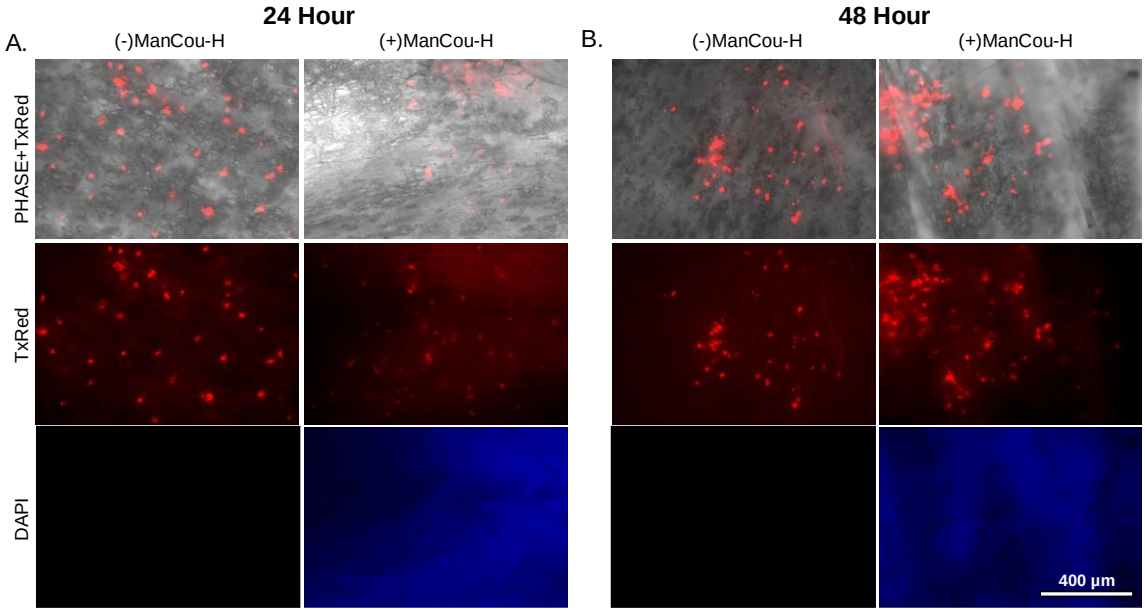

Figure 10 MDA-MB-231 cells in cell tracker red seeded on aligned scaffolds and imaged in phase, TxRed, and DAPI. (A) 24 hours with and without 20μM ManCou-H media (B) 48 hours with and without 20μM ManCou-H media. Images captured at 10x magnification. DAPI images in conditions without ManCou-H were not taken.

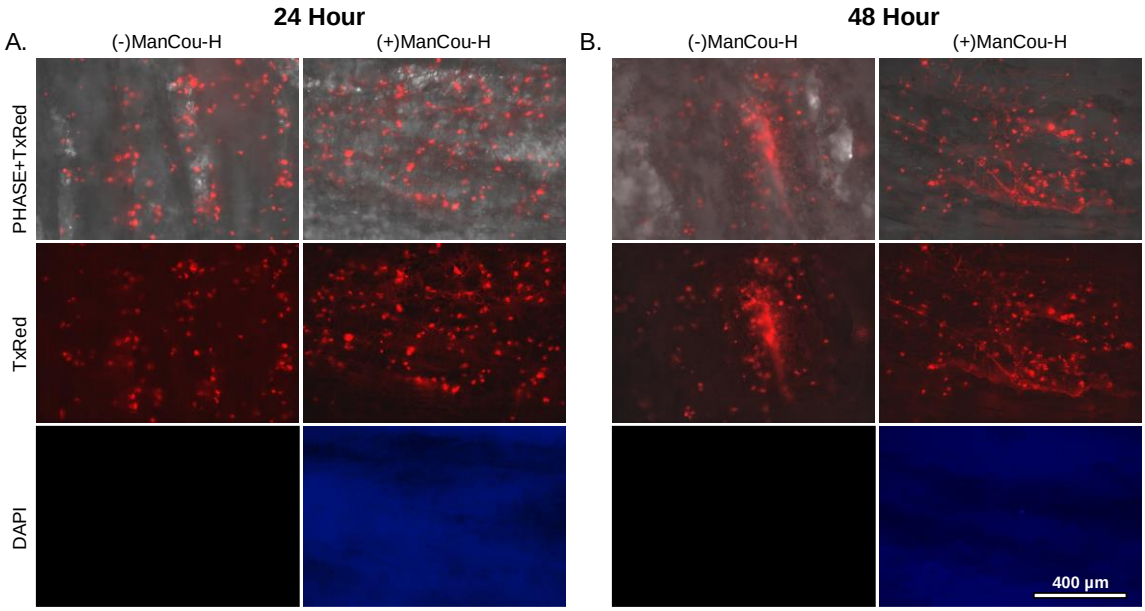

Figure 11 MDA-MB-231 cells in cell tracker red seeded on honeycomb scaffolds and imaged in phase, TxRed, and DAPI. (A) 24 hours with and without 20µM ManCou-H media (B) 48 hours with and without 20µM ManCou-H media. Images captured at 10x magnification. DAPI images in conditions without ManCou-H were not taken.

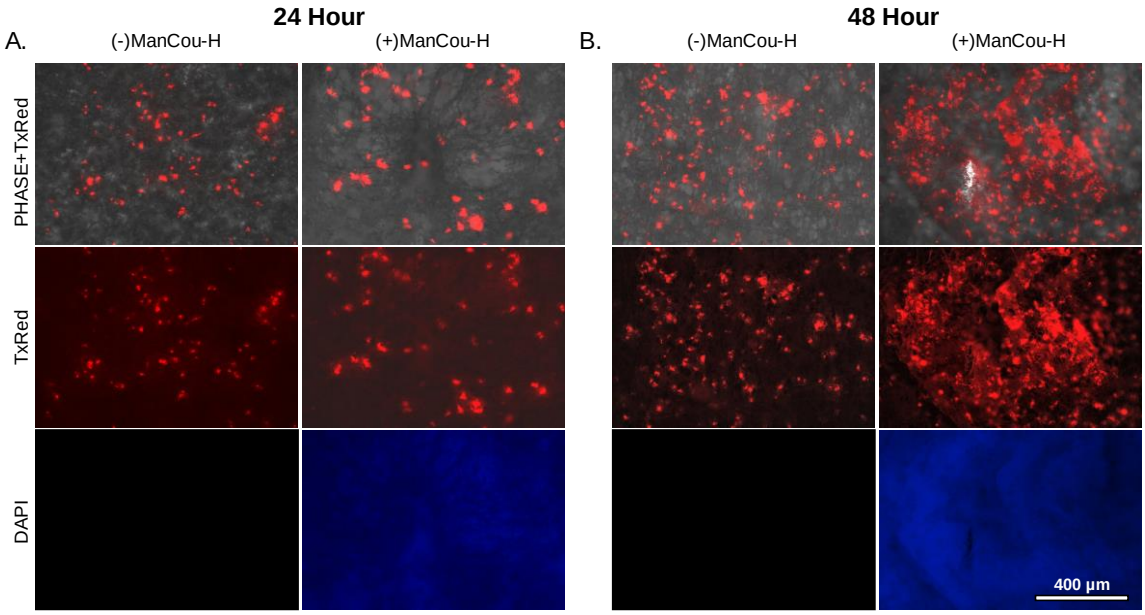

Figure 12 MDA-MB-231 cells in cell tracker red seeded on mesh scaffolds and imaged in phase, TxRed, and DAPI. (A) 24 hours with and without 20μM ManCou-H media (B) 48 hours with and without 20μM ManCou-H media. Images captured at 10x magnification. DAPI images in conditions without ManCou-H were not taken.

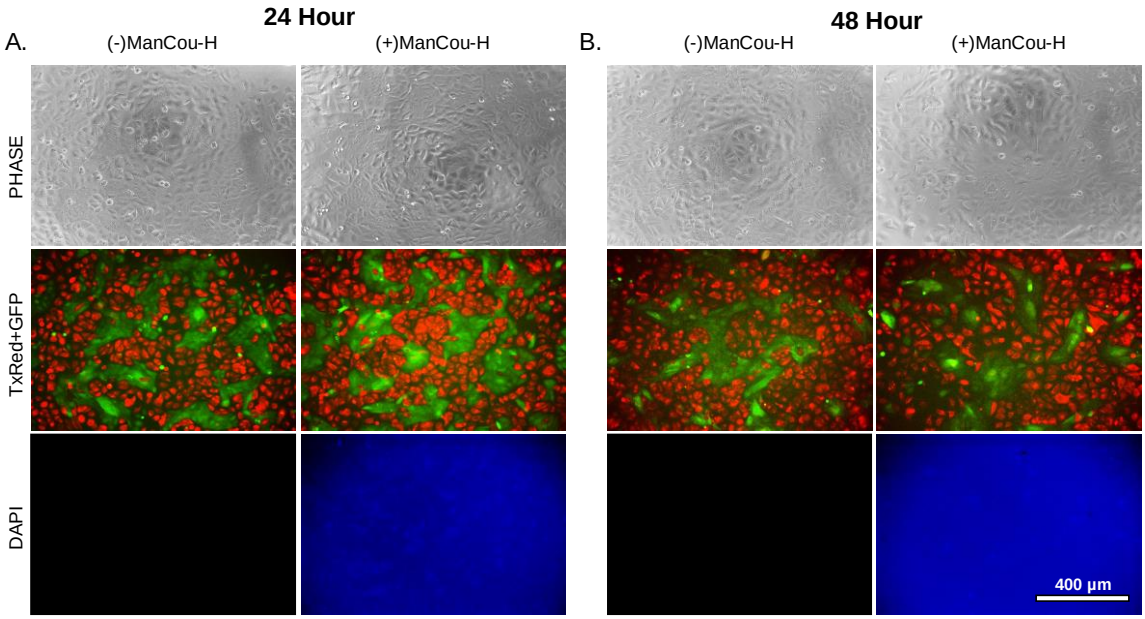

Figure 13 184B5 cells in cell tracker green and MCF7 cells cell tracker red seeded in coculture on 2D culture plate imaged in phase, TxRed and DAPI (A) 24 hours with and without 20μM ManCou-H media (B) 48 hours with and without 20μM ManCou-H media. Images captured at 10x magnification. DAPI images in conditions without ManCou-H were not taken.

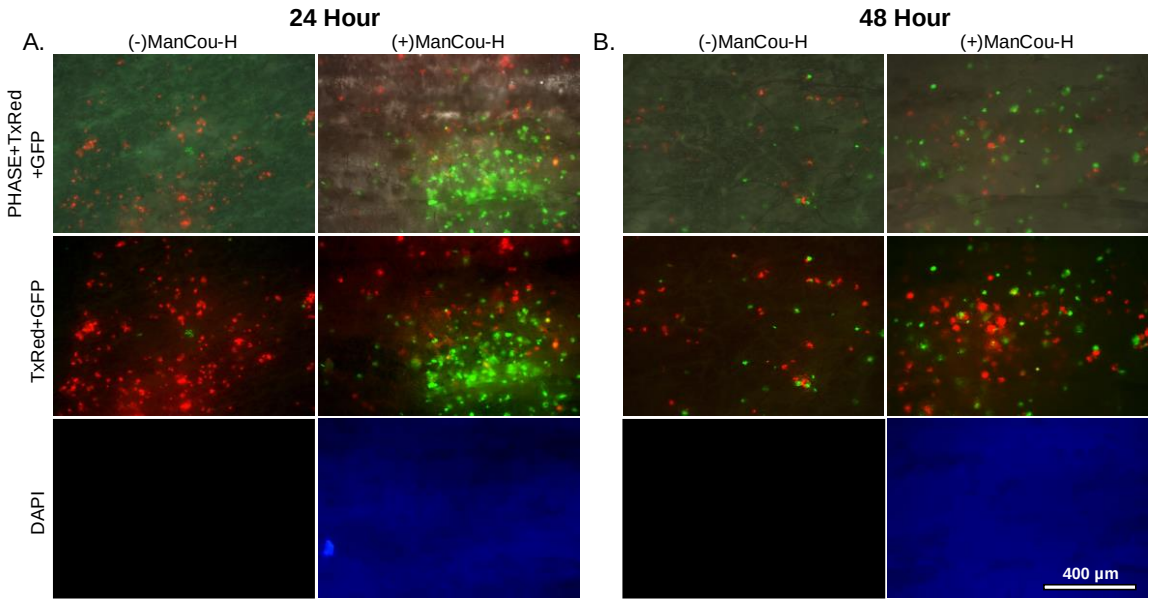

Figure 14 184B5 cells in cell tracker green and MCF7 cells in cell tracker red seeded in coculture on aligned and imaged in phase, TxRed and DAPI (A) 24 hours with and without 20µM ManCou-H media (B) 48 hours with and without 20µM ManCou-H media. Images captured at 10x magnification. DAPI images in conditions without ManCou-H were not taken.

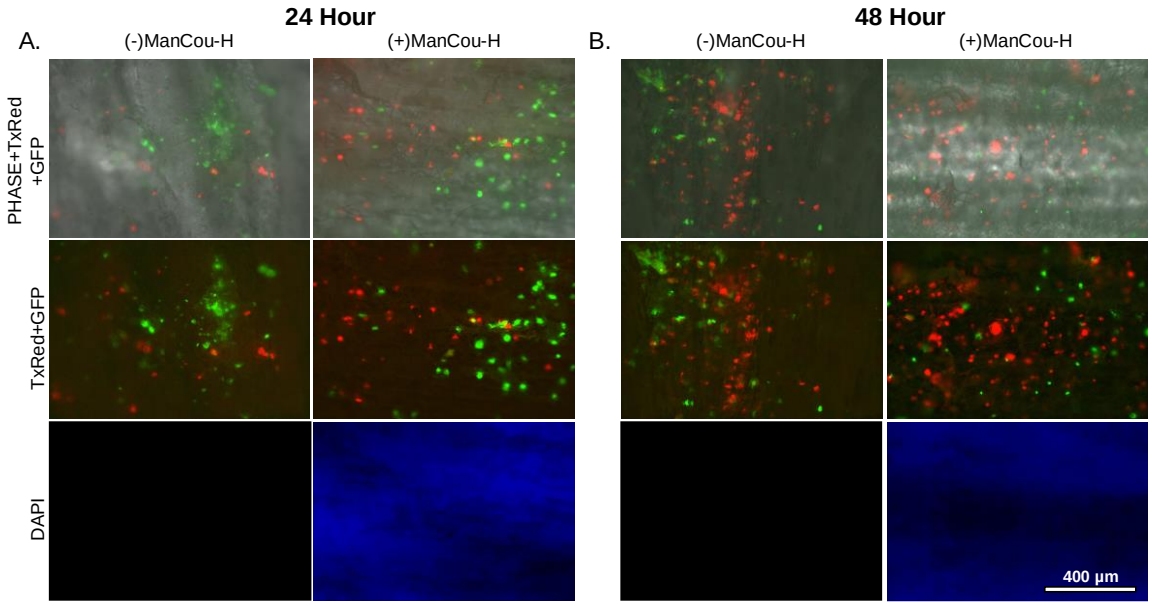

Figure 15 184B5 cells in cell tracker green and MCF7 cells in cell tracker red seeded in coculture on honeycomb and imaged in phase, TxRed and DAPI (A) 24 hours with and without 20μM ManCou-H media (B) 48 hours with and without 20μM ManCou-H media. Images captured at 10x magnification. DAPI images in conditions without ManCou-H were not taken.

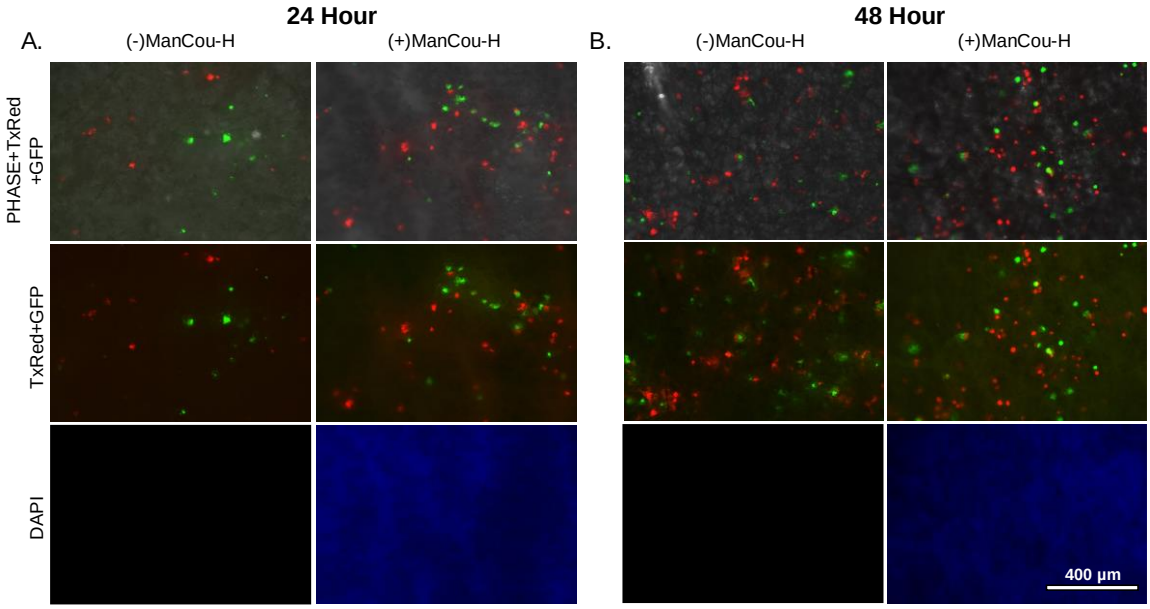

Figure 16 184B5 cells in cell tracker green and MCF7 cells in cell tracker red seeded in coculture on mesh and imaged in phase, TxRed and DAPI (A) 24 hours with and without 20μM ManCou-H media (B) 48 hours with and without 20μM ManCou-H media. Images captured at 10x magnification. DAPI images in conditions without ManCou-H were not taken.

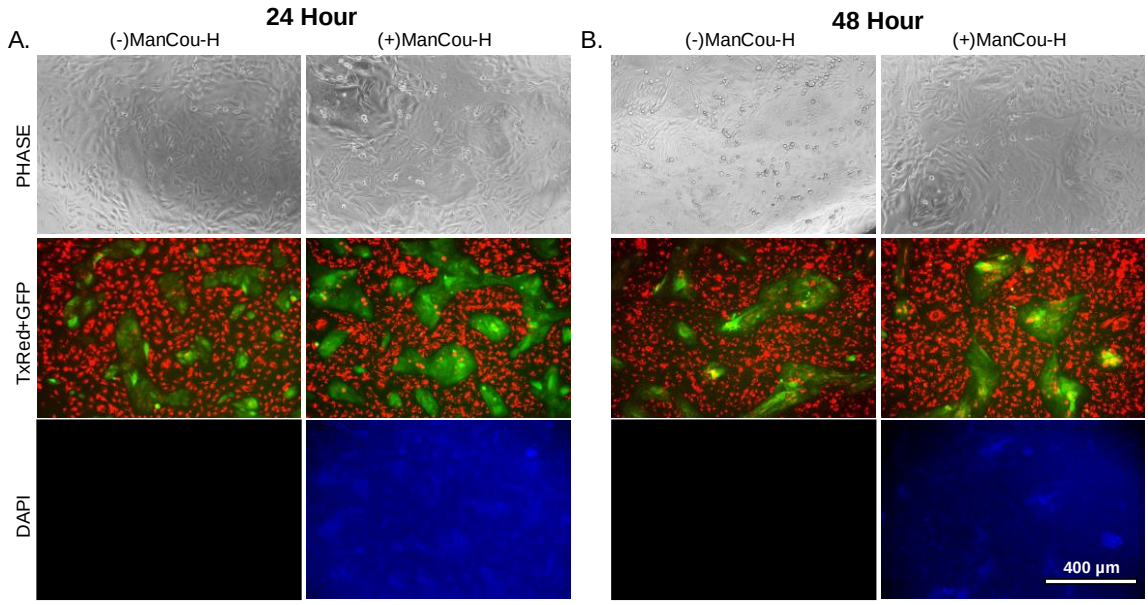

Figure 17 184B5 cells in cell tracker green and MDA-MB-231 cells in cell tracker red seeded in coculture on 2D culture plate imaged in phase, TxRed and DAPI (A) 24 hours with and without 20µM ManCou-H media (B) 48 hours with and without 20µM ManCou-H media. Images captured at 10x magnification. DAPI images in conditions without ManCou-H were not taken.

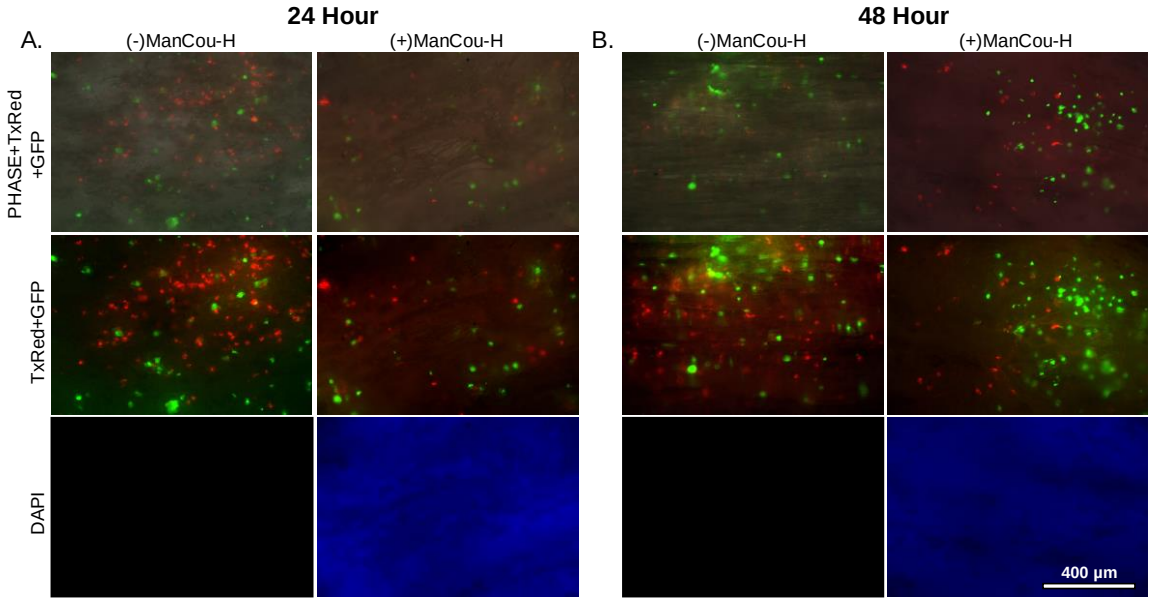

Figure 18 184B5 cells in cell tracker green and MDA-MB-231 cells in cell tracker red seeded in coculture on alignedand imaged in phase, TxRed and DAPI (A) 24 hours with and without 20μM ManCou-H media (B) 48 hours with and without 20μM ManCou-H media. Images captured at 10x magnification. DAPI images in conditions without ManCou-H were not taken.

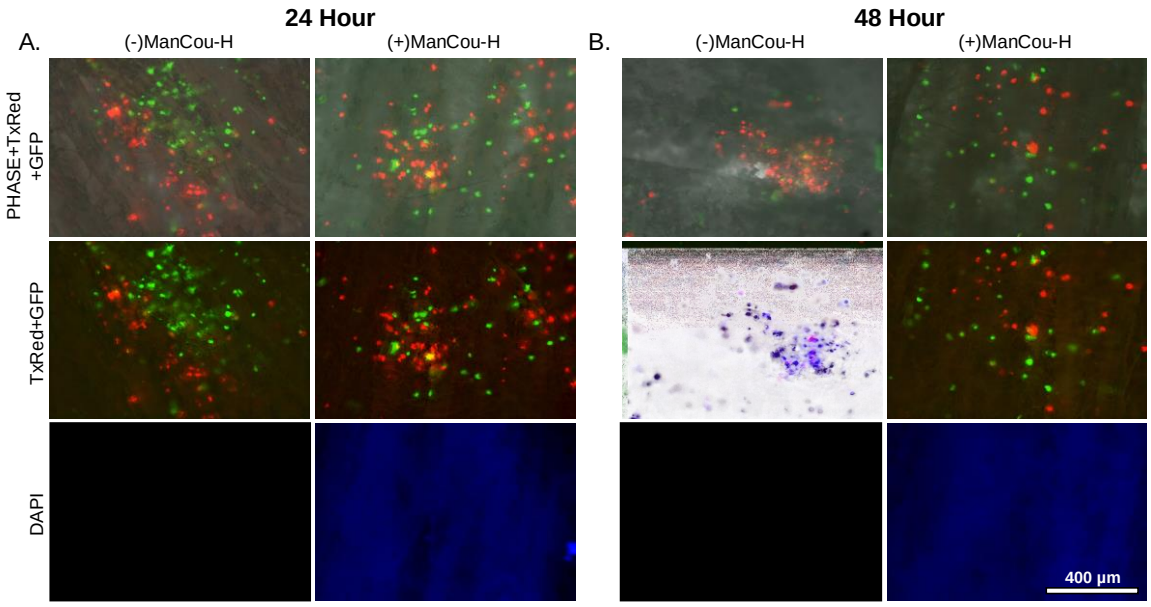

Figure 19 184B5 cells in cell tracker green and MDA-MB-231 cells in cell tracker red seeded in coculture on honeycomb and imaged in phase, TxRed and DAPI (A) 24 hours with and without 20μM ManCou-H media (B) 48 hours with and without 20μM ManCou-H media. Images captured at 10x magnification. DAPI images in conditions without ManCou-H were not taken.

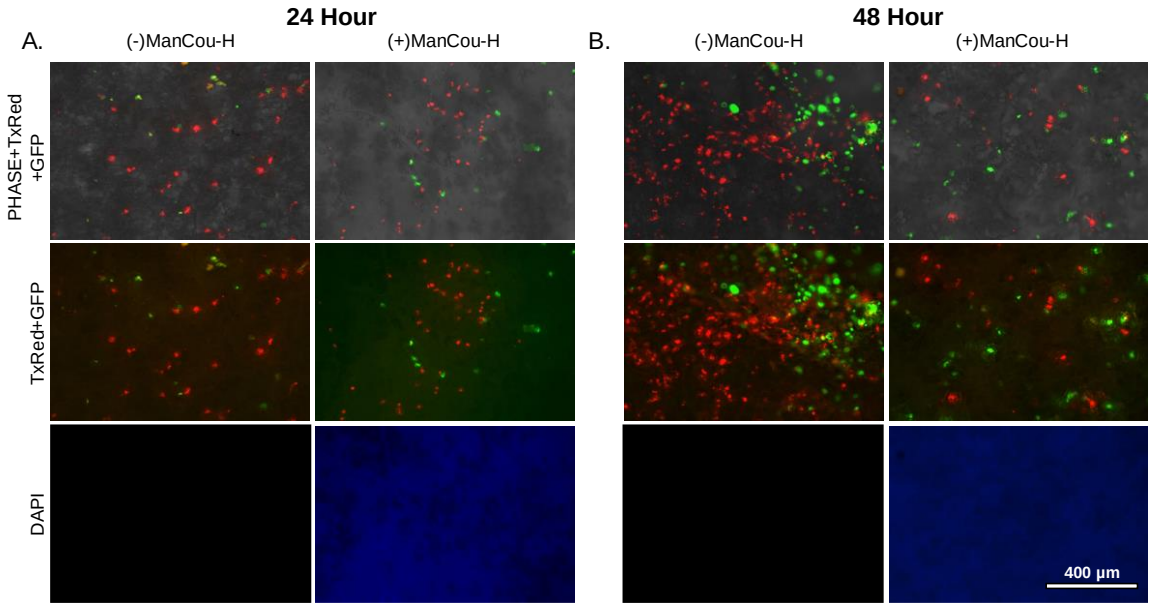

Figure 20 184B5 cells in cell tracker green and MDA-MB-231 cells in cell tracker red seeded in coculture on mesh and imaged in phase, TxRed and DAPI (A) 24 hours with and without 20µM ManCou-H media (B) 48 hours with and without 20µM ManCou-H media. Images captured at 10x magnification. DAPI images in conditions without ManCou-H were not taken.

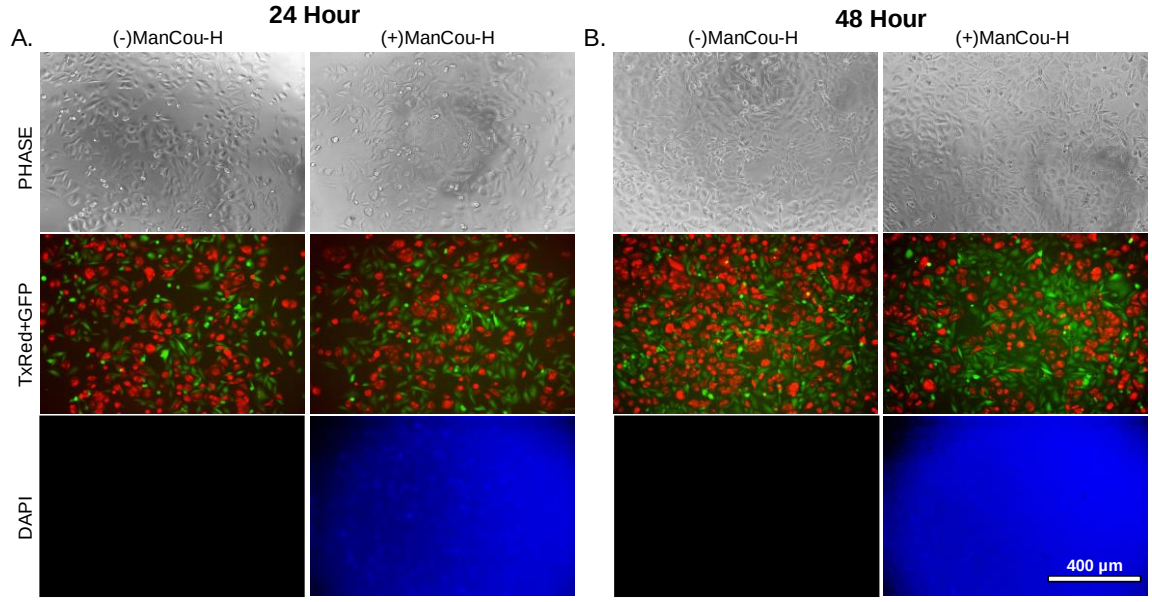

Figure 21 MDA-MB-231 cells in cell tracker green and MCF7 cells in cell tracker red seeded in coculture on 2D culture plate imaged in phase, TxRed and DAPI (A) 24 hours with and without 20μM ManCou-H media (B) 48 hours with and without 20μM ManCou-H media. Images captured at 10x magnification. DAPI images in conditions without ManCou-H were not taken.

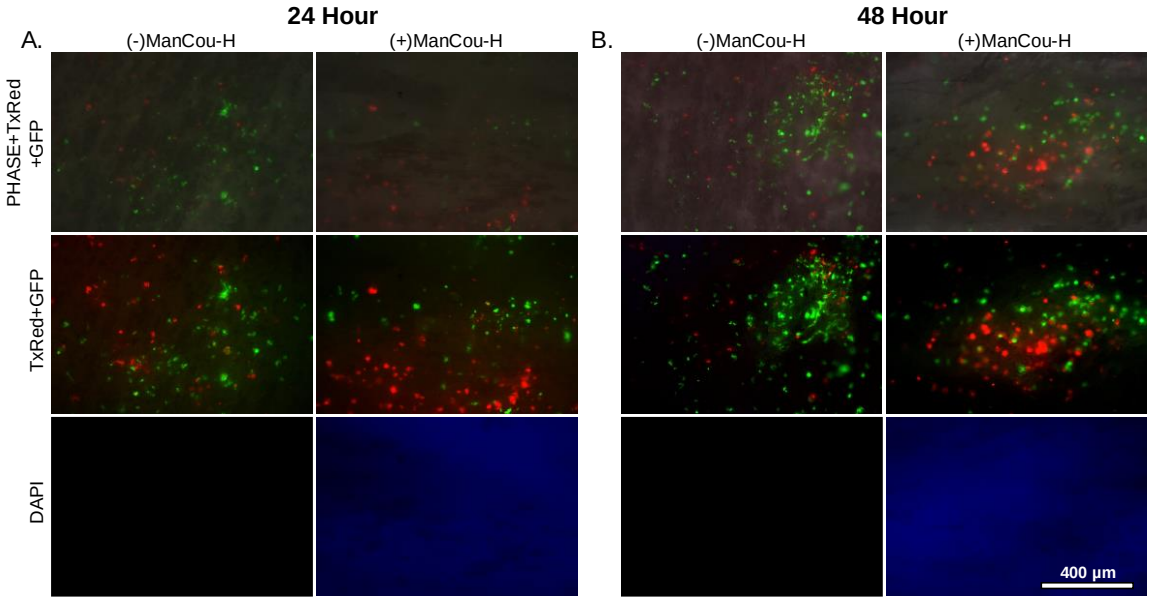

Figure 22 MDA-MB-231 cells in cell tracker green and MCF7 cells in cell tracker red seeded in coculture on aligned and imaged in phase, TxRed and DAPI (A) 24 hours with and without 20μM ManCou-H media (B) 48 hours with and without 20μM ManCou-H media. Images captured at 10x magnification. DAPI images in conditions without ManCou-H were not taken.

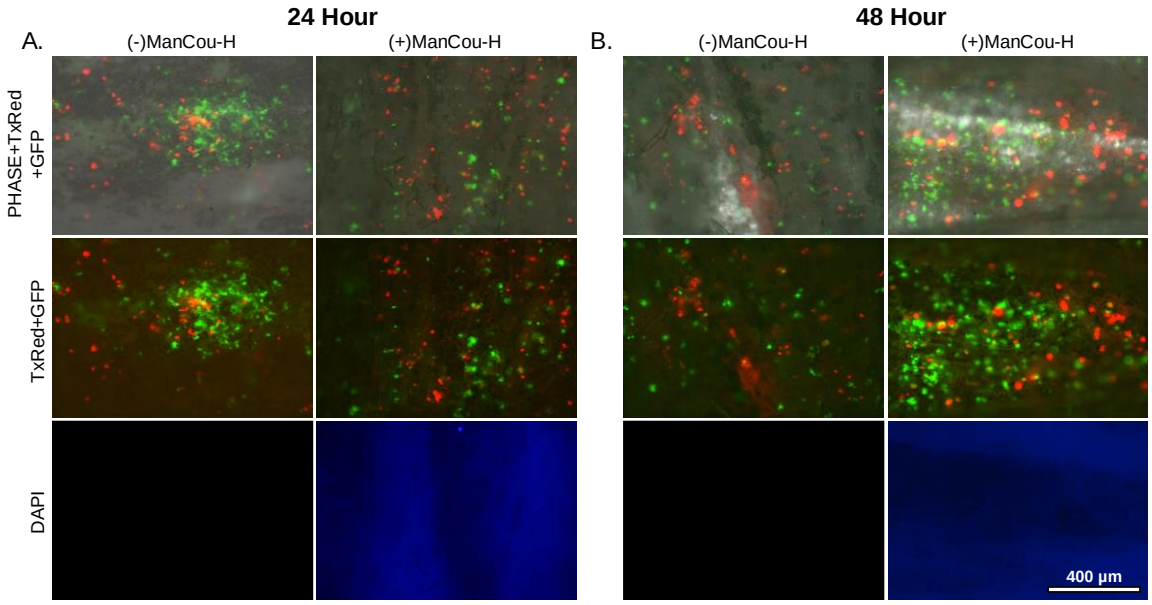

Figure 23 MDA-MB-231 cells in cell tracker green and MCF7 cells in cell tracker red seeded in coculture on honeycomb and imaged in Phase, TxRed and DAPI (A) 24 hours with and without 20µM ManCou-H media (B) 48 hours with and without 20µM ManCou-H media. Images captured at 10x magnification. DAPI images in conditions without ManCou-H were not taken.

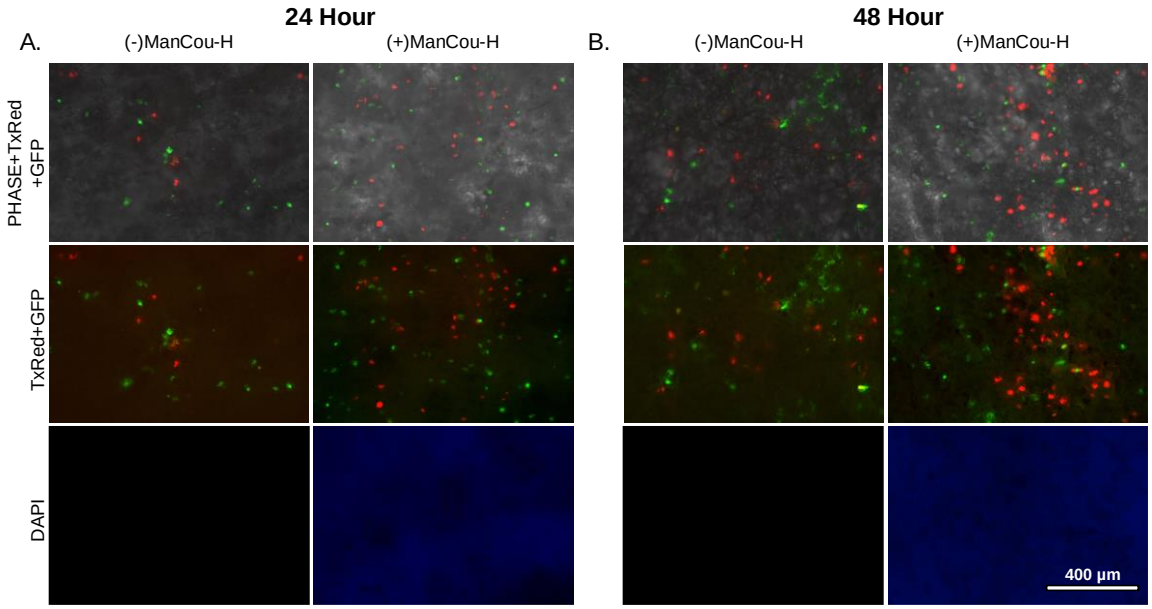

Figure 24 MDA-MB-231 cells in cell tracker green and MCF7 cells in cell tracker red seeded in coculture on mesh and imaged in phase, TxRed and DAPI (A) 24 hours with and without 20μM ManCou-H media (B) 48 hours with and without 20μM ManCou-H media. Images captured at 10x magnification. DAPI images in conditions without ManCou-H were not taken.

In general, cells seeded on 2D culture plates appear to aggregate more in clusters both in the single cell lines as well as the cocultures. On all scaffold types, cells appear to spread out more in single cells as well as clusters. In cells that have been seeded on 2D culture plates and incubated in ManCou-H media, the DAPI filter shows some uptake of probe more so after 24h and less so after 48h. This observation is consistent with MCF7 and MDA-MB-231 (Figure 5 and Figure 9). 184B5 shows little to no uptake in the DAPI filter as was expected (Figure 1). In cells seeded on scaffolds, there was no visible ManCou-H uptake across all 3 cell lines and across all scaffold types (Figures 2-4, 6-8, and 10-12). Finally, cocultures seeded on 2D culture plates appear to be more intertwined with the differing cell populations (Figures 13, 17, 21), but on scaffolds, cell populations appear to segregate themselves from one another (Figures 14-16, 18-20, 22-24).

3.2 GLUT5 expression in 2D vs 3D environment

In order to identify any differences in GLUT5 expression between traditional culture plates and the PCL scaffolds, 184B5, MCF7, and MDA-MB-231 were seeded at a density of 3,000 cells and were placed in either supplemented RPMI 1640 culture media or ManCou-H containing media for 24h and 48h. Cells were fixed and immunocytochemistry was performed specifically targeting GLUT5. Images were taken at both 10x and 20x magnification in the phase and GFP channels and were enhanced individually using ImageJ in order to visualize GLUT5. Separate 10x images were taken using identical settings in order to provide quantitative data of GLUT5 intensity between cells seeded on culture plates and on scaffolds.

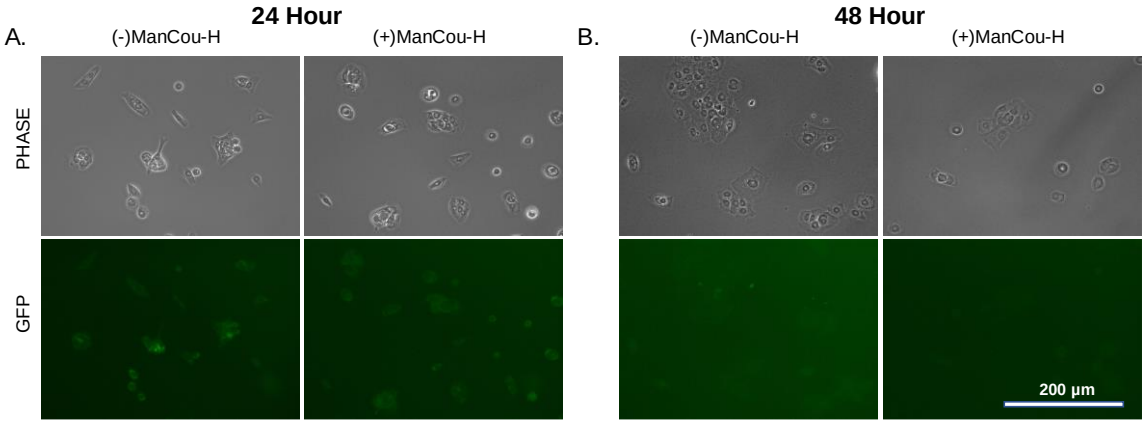

Figure 25 184B5 cells seeded on 2D culture plates and immuno-stained for GLUT5 imaged in phase and GFP (A) 24 hours with and without 20μM ManCou-H media

(B) 48 hours with and without 20μM ManCou-H media. Images captured at 20x magnification.

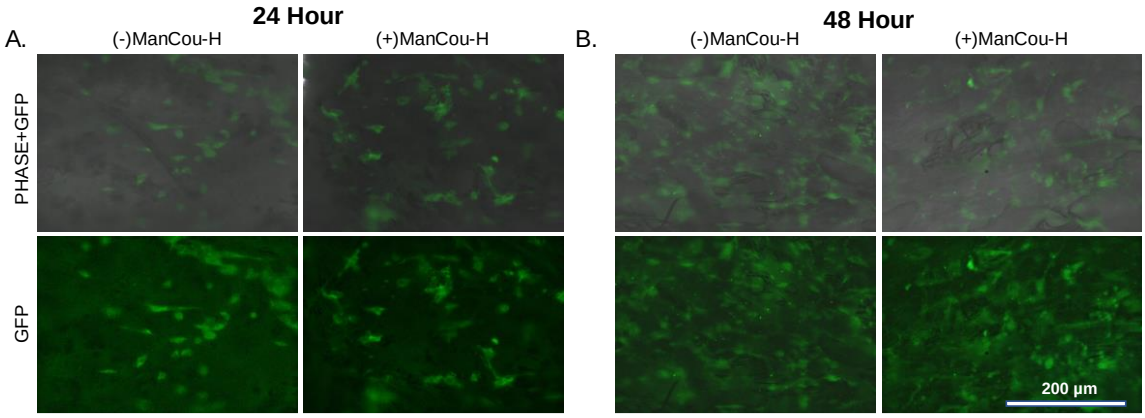

Figure 26 184B5 cells seeded on aligned scaffolds and immuno-stained for GLUT5. Imaged in phase and GFP (A) 24 hours with and without 20μM ManCou-H media (B) 48 hours with and without 20μM ManCou-H media. Images captured at 20x magnification.

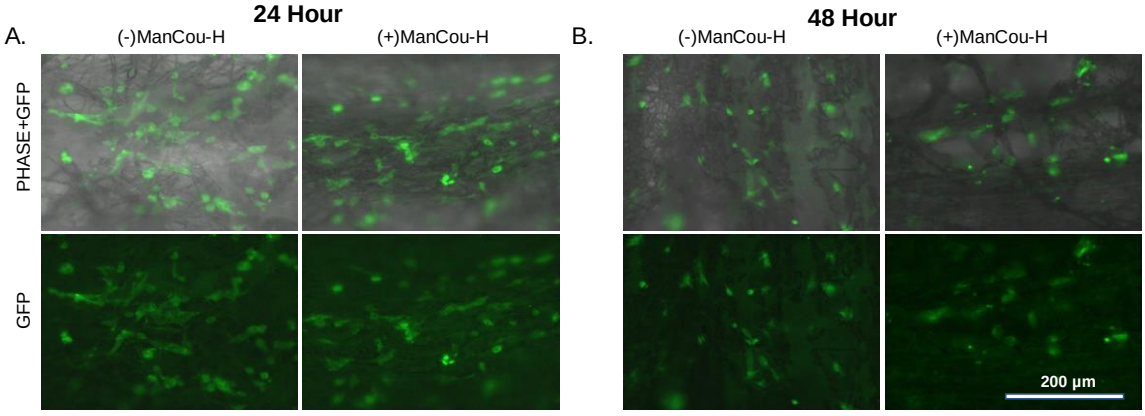

Figure 27 184B5 cells seeded on honeycomb scaffolds and immuno-stained for GLUT5. Imaged in phase and GFP (A) 24 hours with and without 20μM ManCou-H media (B) 48 hours with and without 20μM ManCou-H media. Images captured at 20x magnification.

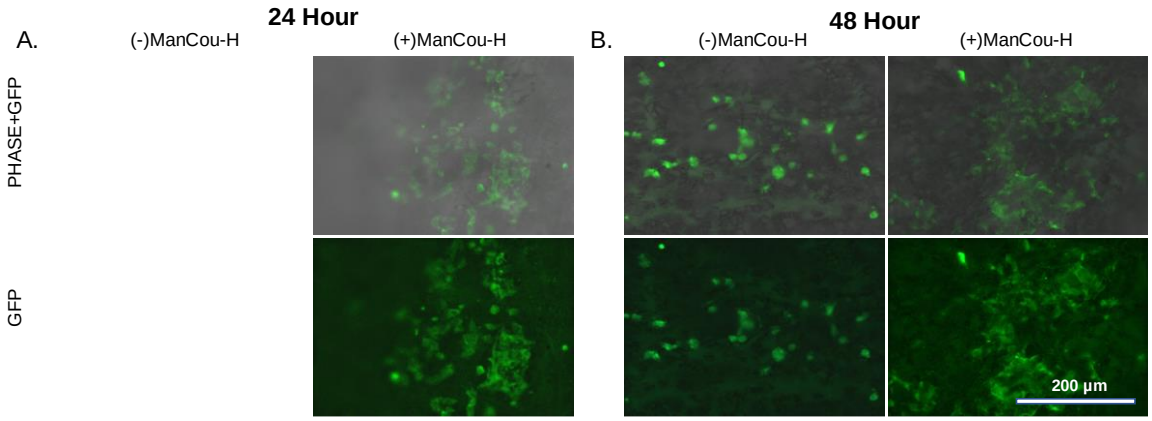

Figure 28 184B5 cells seeded on mesh scaffolds and immuno-stained for GLUT5. Imaged in phase and GFP (A) 24 hours with and without 20µM ManCou-H media (B) 48 hours with and without 20µM ManCou-H media. Images captured at 20x magnification.

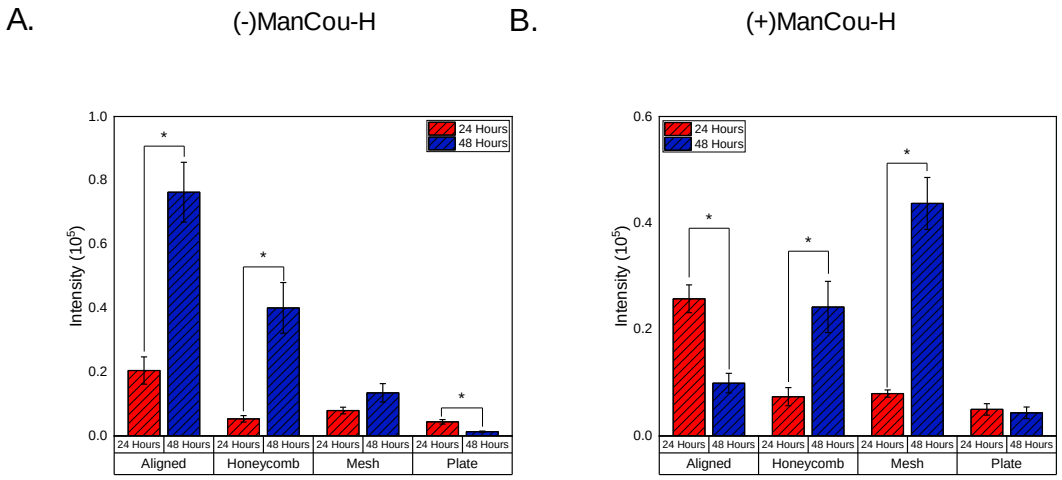

Figure 29 Intensity of 184B5 cells stained against GLUT5 antibody on aligned, honeycomb, mesh scaffolds as well as the 2D culture plate after 24h and 48h in (A) regular culture media, and (B) in ManCou-H containing media. Cell seeding density was maintained across all groups. Error bars represent the standard error of mean.

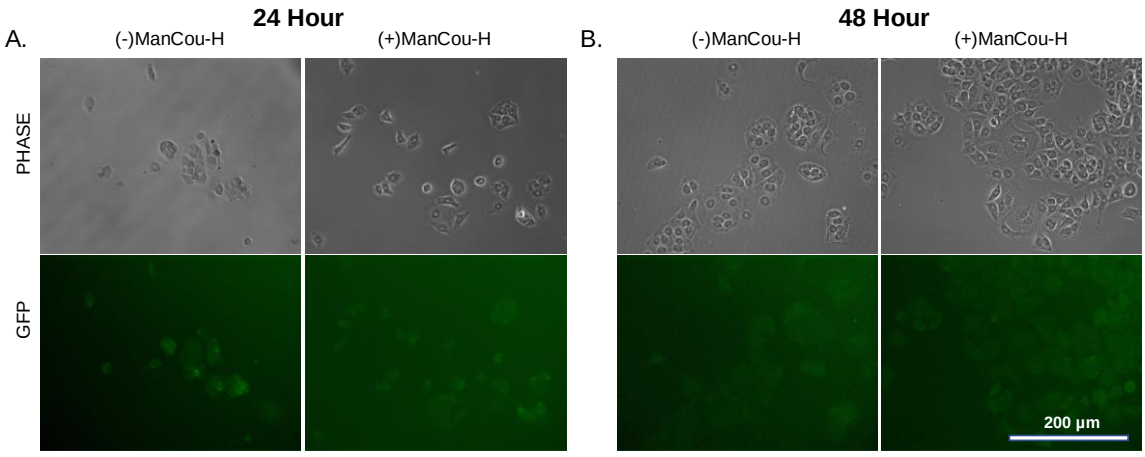

Figure 30 MCF7 cells seeded on 2D culture plates and immuno-stained for GLUT5 imaged in phase and GFP (A) 24 hours with and without 20µM ManCou-H media (B) 48 hours with and without 20µM ManCou-H media. Images captured at 20x magnification.

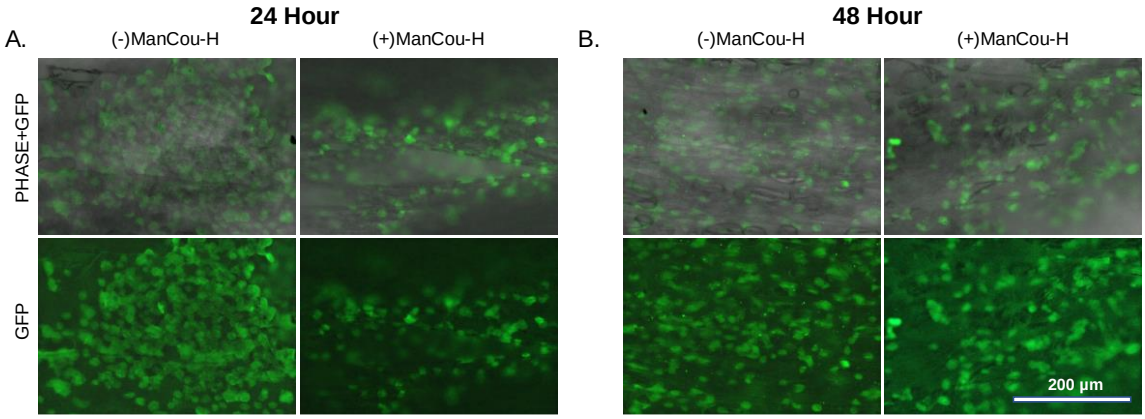

Figure 31 MCF7 cells seeded on aligned scaffolds and immuno-stained for GLUT5. Imaged in phase and GFP (A) 24 hours with and without 20µM ManCou-H media (B) 48 hours with and without 20µM ManCou-H media. Images captured at 20x magnification.

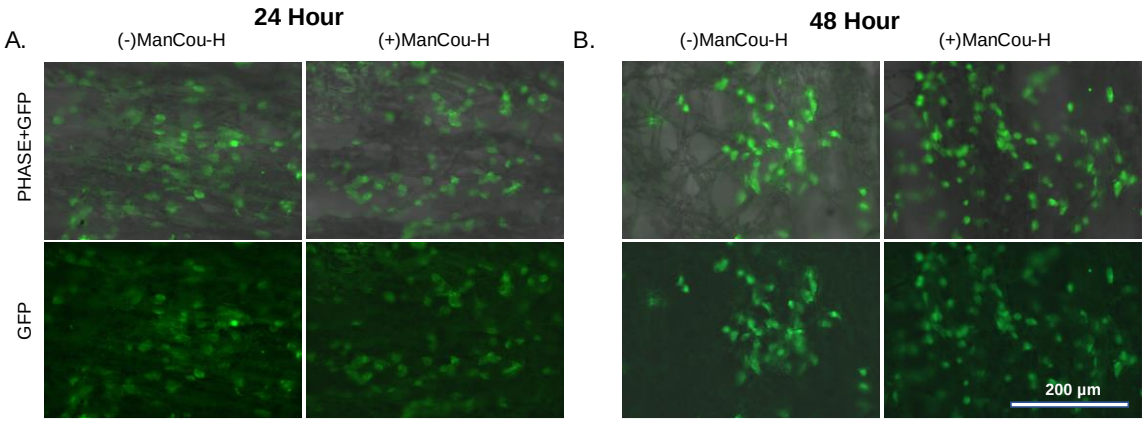

Figure 32 MCF7 cells seeded on honeycomb scaffolds and immuno-stained for GLUT5. Imaged in phase and GFP (A) 24 hours with and without 20µM ManCou-H media (B) 48 hours with and without 20µM ManCou-H media. Images captured at 20x magnification.

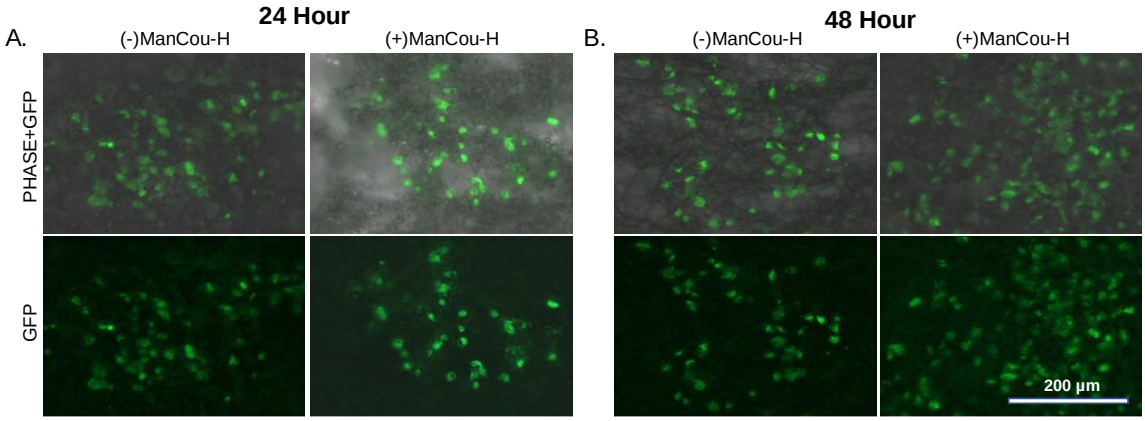

Figure 33 MCF7 cells seeded on mesh scaffolds and immuno-stained for GLUT5. Imaged in phase and GFP (A) 24 hours with and without 20µM ManCou-H media (B) 48 hours with and without 20µM ManCou-H media. Images captured at 20x magnification.

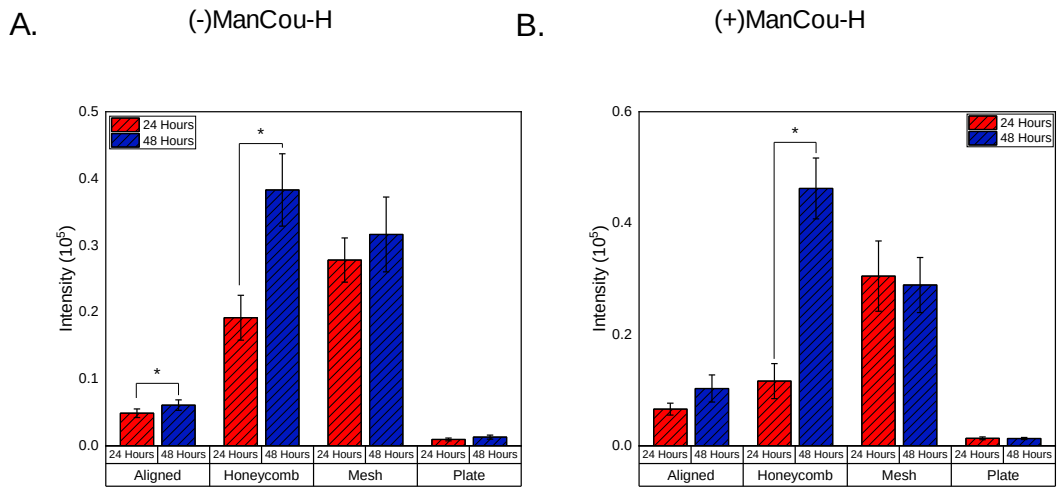

Figure 34 Intensity of MCF7 cells stained against GLUT5 antibody on aligned, honeycomb, mesh scaffolds as well as the 2D culture plate after 24h and 48h in (A) regular culture media, and (B) in ManCou-H containing media. Cell seeding density was maintained across all groups. Error bars represent the standard error of mean.

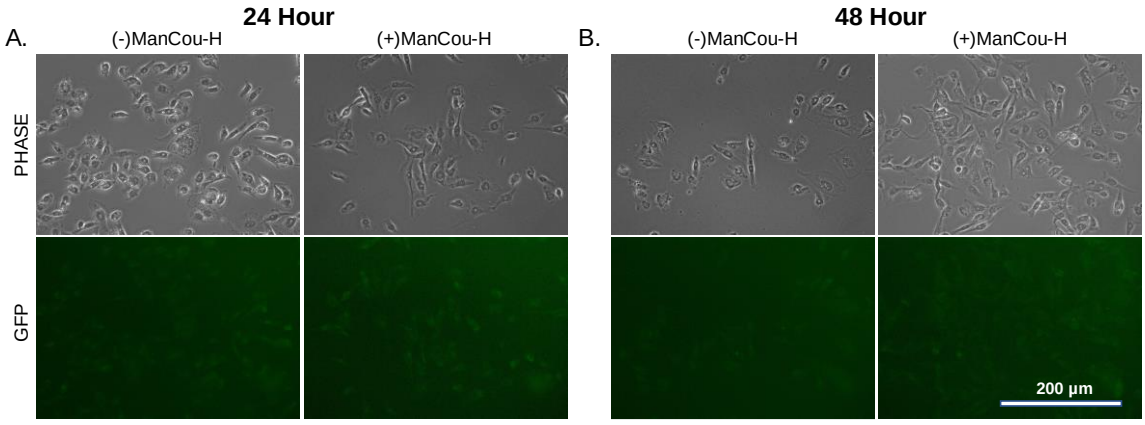

Figure 35 MDA-MB-231 cells seeded on culture plates and immuno-stained for GLUT5 imaged in phase and GFP (A) 24 hours with and without 20µM ManCou-H media (B) 48 hours with and without 20µM ManCou-H media. Images captured at 20x magnification.

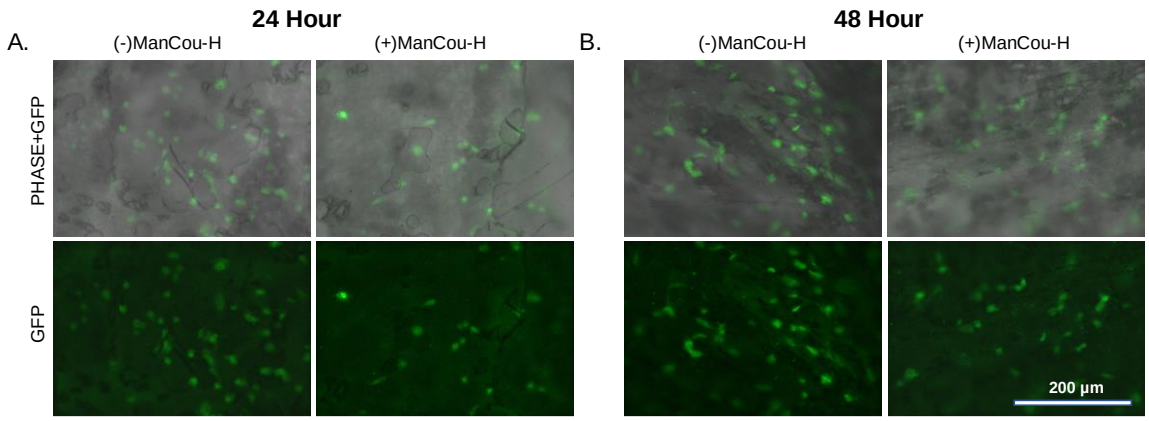

Figure 36 MDA-MB-231 cells seeded on aligned scaffolds and immuno-stained for GLUT5. Imaged in phase and GFP (A) 24 hours with and without 20µM ManCou-H media (B) 48 hours with and without 20µM ManCou-H media. Images captured at 20x magnification.

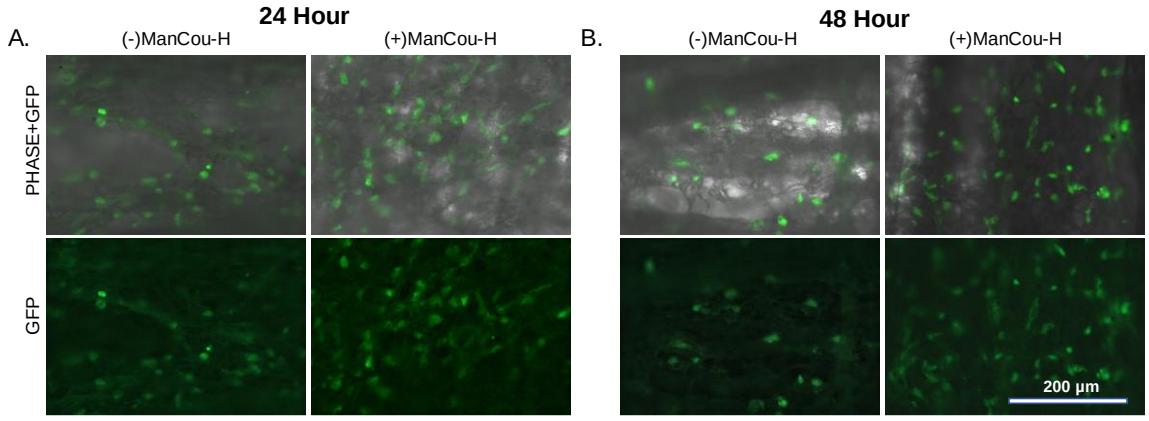

Figure 37 MDA-MB-231 cells seeded on honeycomb scaffolds and immuno-stained for GLUT5. Imaged in phase and GFP (A) 24 hours with and without 20µM ManCou-H media (B) 48 hours with and without 20µM ManCou-H media. Images captured at 20x magnification.

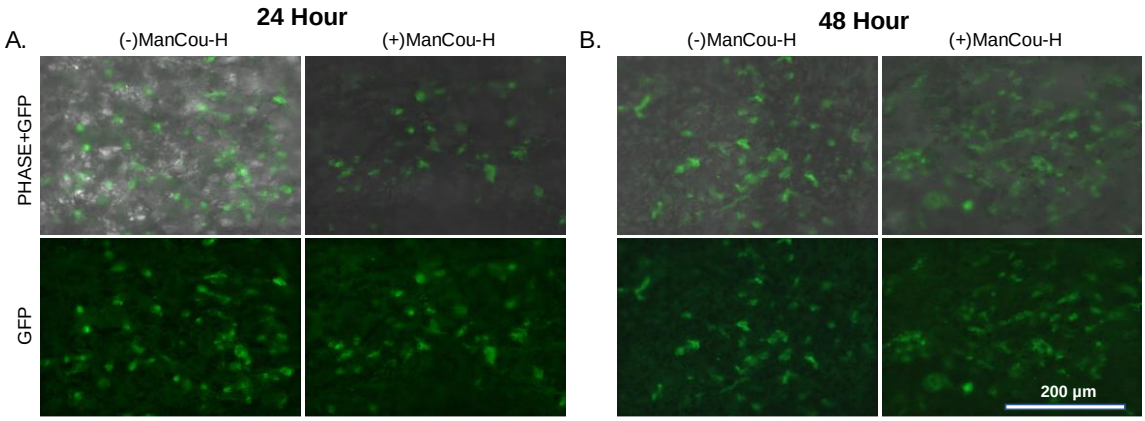

Figure 38 MDA-MB-231 cells seeded on mesh scaffolds and immuno-stained for GLUT5. Imaged in phase and GFP (A) 24 hours with and without 20µM ManCou-H media (B) 48 hours with and without 20µM ManCou-H media. Images captured at 20x magnification.

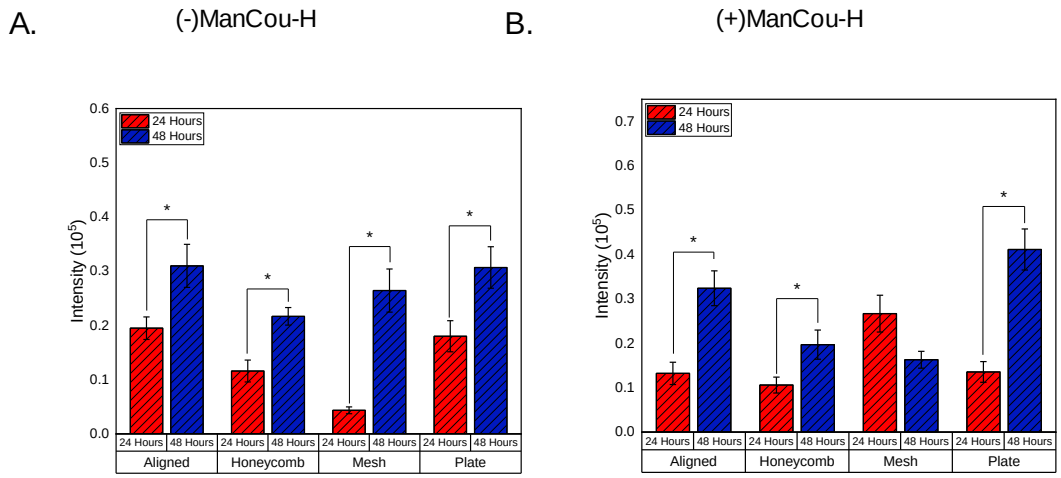

Figure 39 Intensity of MDA-MB-231 cells stained against GLUT5 antibody on aligned, honeycomb, mesh scaffolds as well as the 2D culture plate after 24h and 48h in (A) regular culture media, and (B) in ManCou-H containing media. Cell seeding density was maintained across all groups. Error bars represent the standard error of mean.

In Figure 25, Figure 30 and Figure 35, GLUT5 intensity in 184B5, MCF7, and MDA-MB-231 cells seeded on 2D culture plate is faint. There is an increase in intensity in GLUT5 in all cell types seeded on scaffolds (Figures 26-28, 31-33, 36-38). Figure 28 does not have images for 184B5 cells on mesh scaffolds at 24h without probe, and due to the recent campus shutdown, images were not able to be taken and therefore they are not included in the figure.

The previous observations are consistent with the quantitative data obtained using ImageJ software. In Figure 29 184B5 cells show an increase in GLUT5 intensity from 24h to 48h in all scaffold types except mesh when ManCou-H probe is absent. When ManCou-H is present there is an increase in GLUT5 intensity from 24h to 48h across all scaffold types. The change in GLUT5 intensity in 184B5 cells seeded on plates is minimal in both the treated and non-treated groups.

In Figure 34, MCF7 cells show an increase in GLUT5 intensity in aligned and honeycomb scaffolds from 24h to 48 hours without ManCou-H probe, however in the mesh scaffolds there is a decrease in GLUT5 intensity from 24h to 48h without ManCou-H probe. In all three scaffold types, MCF7 cells on scaffolds in ManCou-H probe have an increase in GLUT5 intensity. Both the treated and non-treated groups of MCF7 cells on 2D culture plates show similar intensity at 24h and 48 hours.

There is an increase in GLUT5 intensity in MDA-MB-231 cells seeded on aligned and mesh scaffolds of non-treated groups after 24h and 48h. The non-treated MDA-MB-231 cells seeded on the honeycomb scaffolds exhibit similar intensity to the cells seeded on the 2D culture plate after 24h and 48h. The treated group shows and increase in GLUT5 intensity in the aligned and honeycomb scaffold types after 24h and 48h. GLUT5 intensity decreases in MDA-MB-231 on mesh scaffolds after 24h. There is minimal change in GLUT5 intensity in MDA-MB-231 cells seeded on 2D culture plates in the treated group.

Generally, cells seeded on the aligned scaffolds have an increased GLUT5 expression after 48h compared to 24h. A similar generalization can be made for the honeycomb scaffold as well. GLUT5 expression begins to differ after 24h and 48h among the mesh scaffold type and remains similar after 24h and 48h on the 2D culture plate.

3.3 Cytokeratin-18 expression 2D vs 3D environment

In order to identify any differences in cytokeratin-18 expression between traditional culture plates and the PCL scaffolds, 184B5, MCF7, and MDA-MB-231 were seeded at a density of 3,000 cells and were placed in either supplemented RPMI 1640 culture media or ManCou-H containing media for 24h and 48h. Cells were fixed and immunocytochemistry was performed specifically targeting cytokeratin-18. NucRed was used to stain the nuclei of individual cells Images were taken at both 10x and 20x magnification in the phase, GFP, and Cy5 channels, and were enhanced individually using ImageJ to visualize cytokeratin-18 intensity. Separate 10x images were taken using identical settings in order to provide quantitative data of cytokeratin-18 intensity between cells seeded on culture plates and on scaffolds.

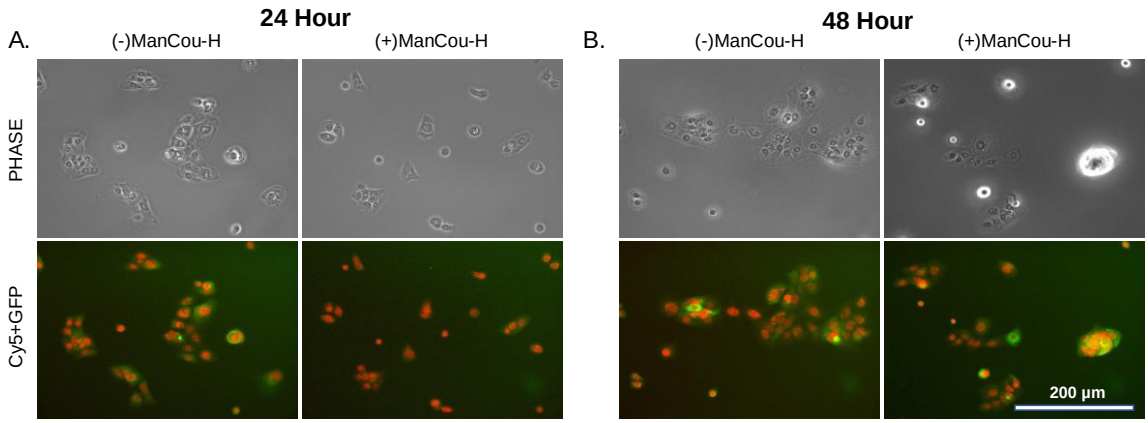

Figure 40 184B5 cells seeded on culture plates and immuno-stained for cytokeratin-18, with the nucleus stained red. Imaged in phase, GFP, and Cy5 (A) 24 hours with and without 20µM ManCou-H media (B) 48 hours with and without 20µM ManCou-H media. Images captured at 20x magnification.

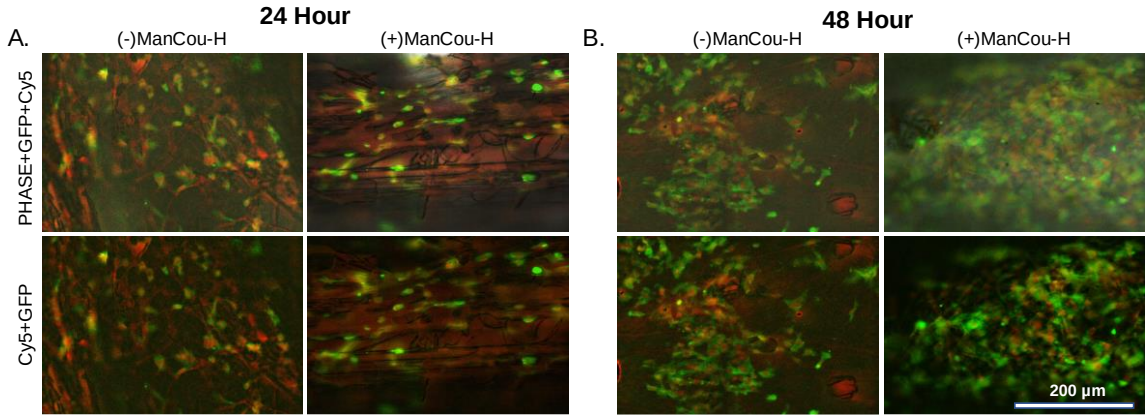

Figure 41 184B5 cells seeded on aligned scaffolds and immuno-stained for cytokeratin-18, with the nucleus stained red. Imaged in phase, GFP and Cy5 (A) 24 hours with and without 20µM ManCou-H media (B) 48 hours with and without 20µM ManCou-H media. Images captured at 20x magnification.

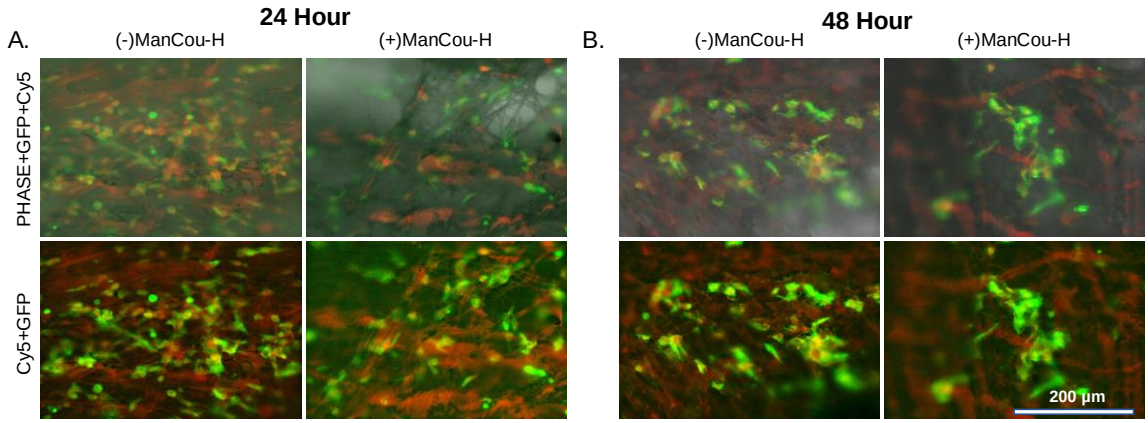

Figure 42 184B5 cells seeded on honeycomb scaffolds and immuno-stained for cytokeratin-18, with the nucleus stained red. Imaged in phase, GFP and Cy5 (A) 24 hours with and without 20µM ManCou-H media (B) 48 hours with and without 20µM ManCou-H media. Images captured at 20x magnification.

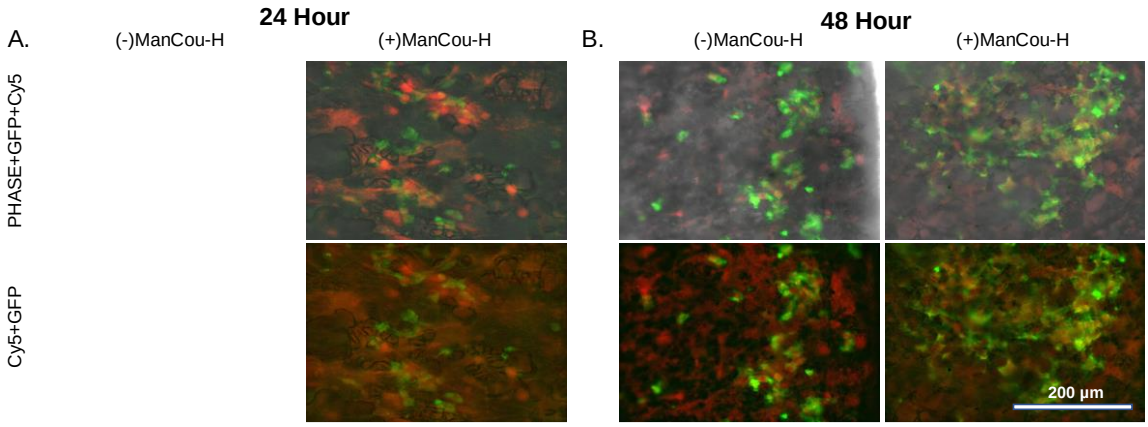

Figure 43 184B5 cells seeded on mesh scaffolds and immuno-stained for cytokeratin-18, with the nucleus stained red. Imaged in phase, GFP and Cy5 (A) 24 hours with and without 20µM ManCou-H media (B) 48 hours with and without 20µM ManCou-H media. Images captured at 20x magnification.

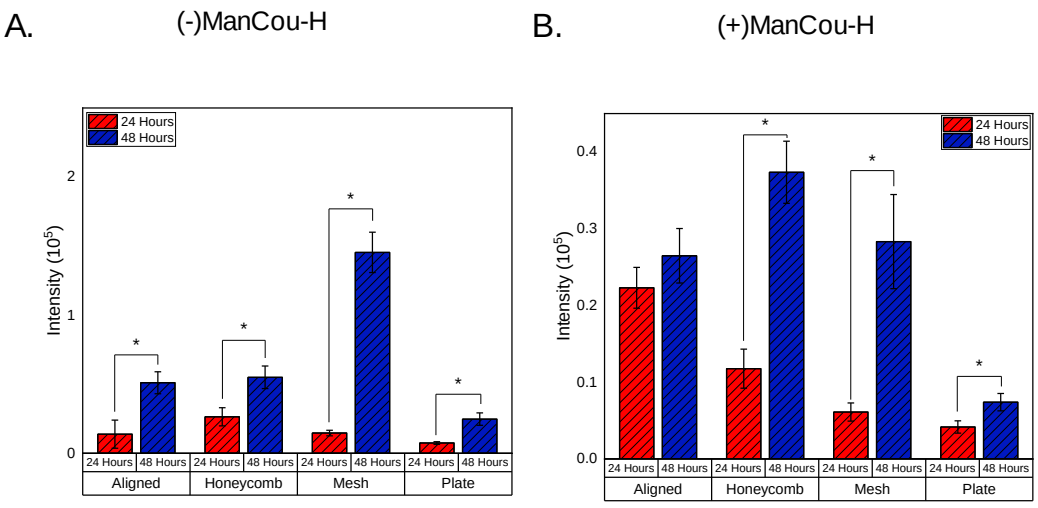

Figure 44 Intensity of 184B5 cells stained against cytokeratin-18 antibody on aligned, honeycomb, mesh scaffolds as well as the 2D culture plate after 24h and 48h in (A) regular culture media, and (B) in ManCou-H containing media. Cell seeding density was maintained across all groups. Error bars represent the standard error of mean.

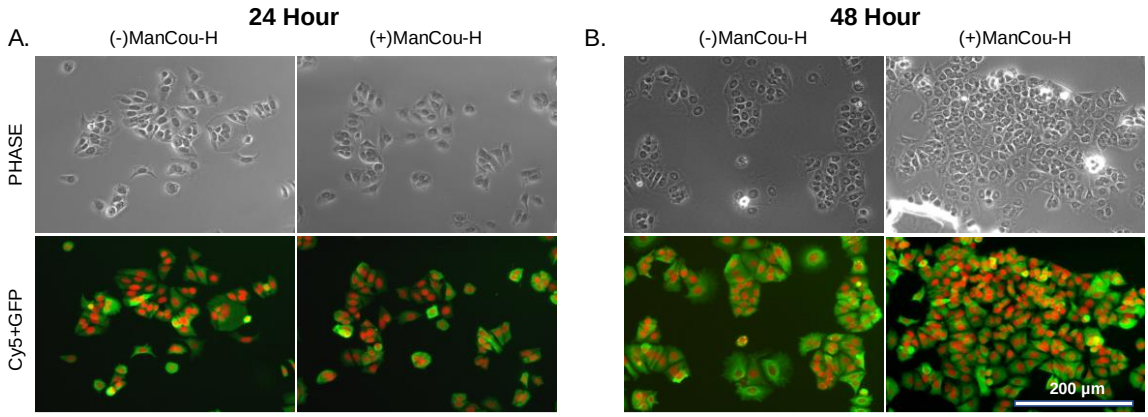

Figure 45 MCF7 cells seeded on culture plates and immuno-stained for cytokeratin-18, with the nucleus stained red. Imaged in phase, GFP and Cy5 (A) 24 hours with and without 20µM ManCou-H media (B) 48 hours with and without 20µM ManCou-H media. Images captured at 20x magnification.

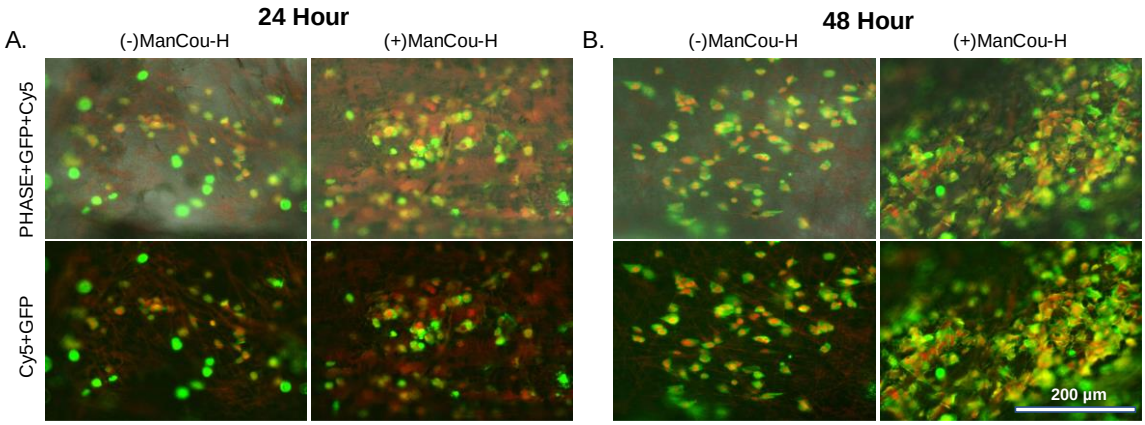

Figure 46 MCF7 cells seeded on aligned scaffolds and immuno-stained for cytokeratin-18, with the nucleus stained red. Imaged in phase, GFP and Cy5 (A) 24 hours with and without 20µM ManCou-H media (B) 48 hours with and without 20µM ManCou-H media. Images captured at 20x magnification.

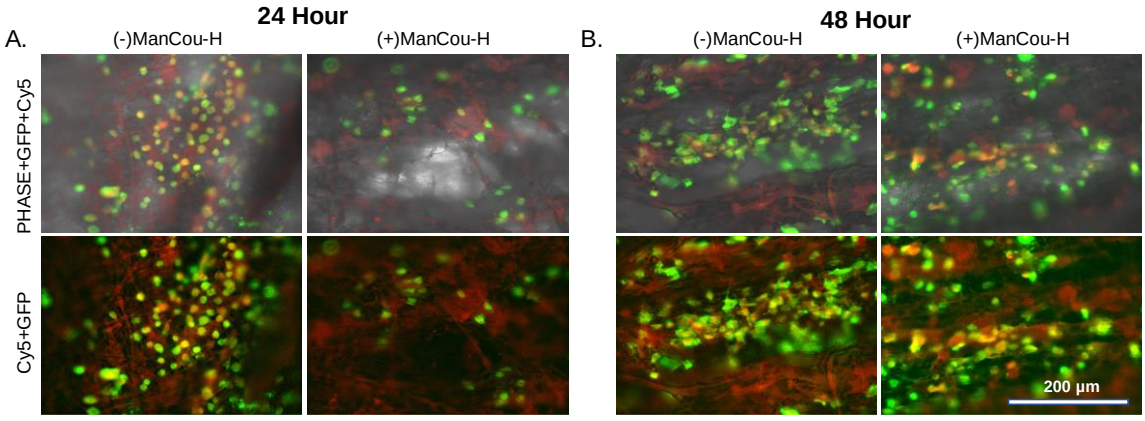

Figure 47 MCF7 cells seeded on honeycomb scaffolds and immuno-stained for cytokeratin-18, with the nucleus stained red. Imaged in phase, GFP and Cy5 (A) 24 hours with and without 20µM ManCou-H media (B) 48 hours with and without 20µM ManCou-H media. Images captured at 20x magnification.

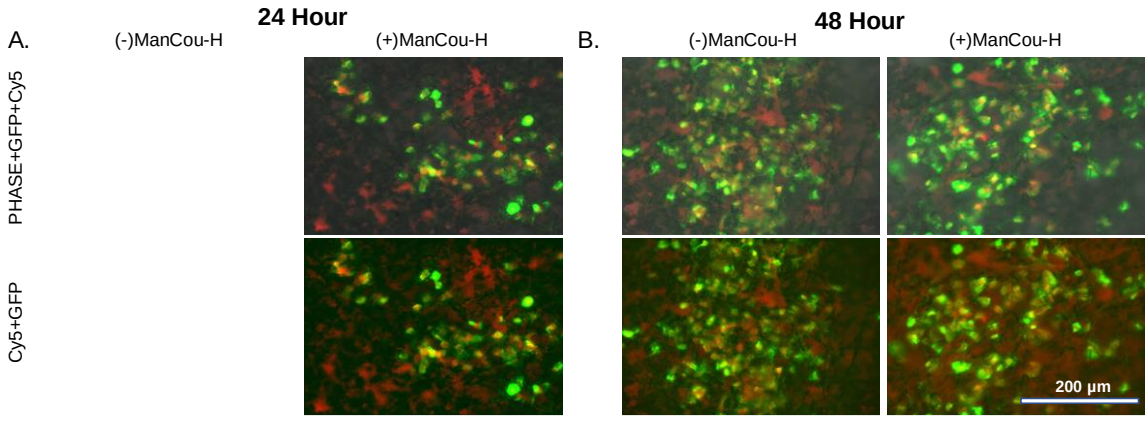

Figure 48 MCF7 cells seeded on mesh scaffolds and immuno-stained for cytokeratin-18, with the nucleus stained red. Imaged in phase, GFP and Cy5 (A) 24 hours with and without 20µM ManCou-H media (B) 48 hours with and without 20µM ManCou-H media. Images captured at 20x magnification.

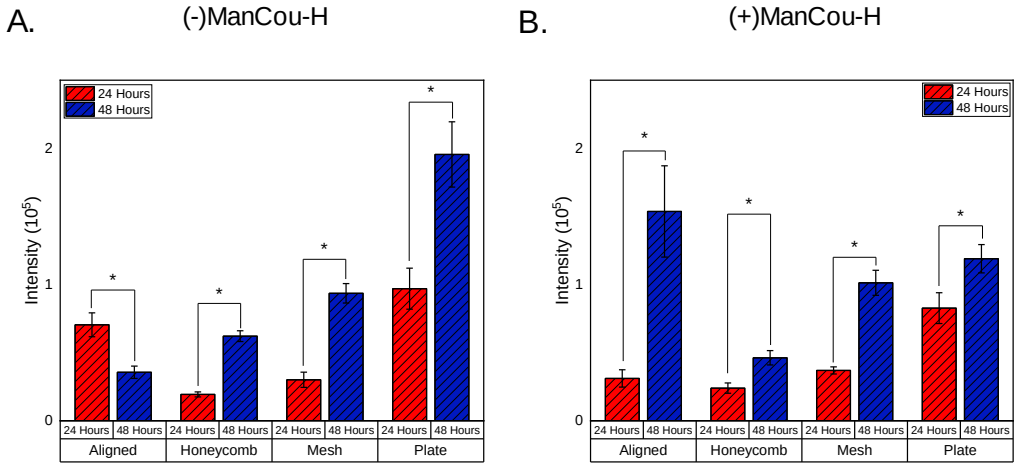

Figure 49 Intensity of MCF7 cells stained against cytokeratin-18 antibody on aligned, honeycomb, mesh scaffolds as well as the 2D culture plate after 24h and 48h in (A) regular culture media, and (B) in ManCou-H containing media. Cell seeding density was maintained across all groups. Error bars represent the standard error of mean.

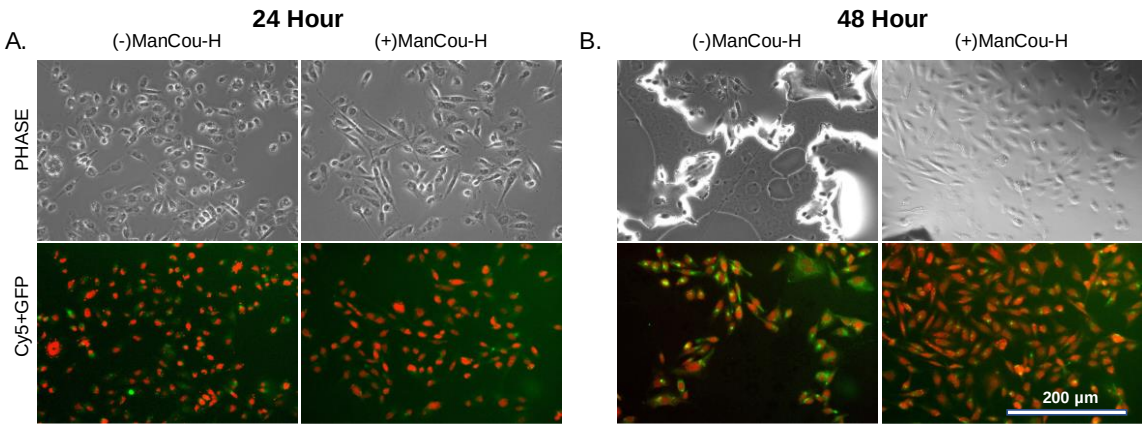

Figure 50 MDA-MB-231 cells seeded on culture plates and immuno-stained for cytokeratin-18, with the nucleus stained red. Imaged in phase, GFP and Cy5 (A) 24 hours with and without 20µM ManCou-H media (B) 48 hours with and without 20µM ManCou-H media. Images captured at 20x magnification.

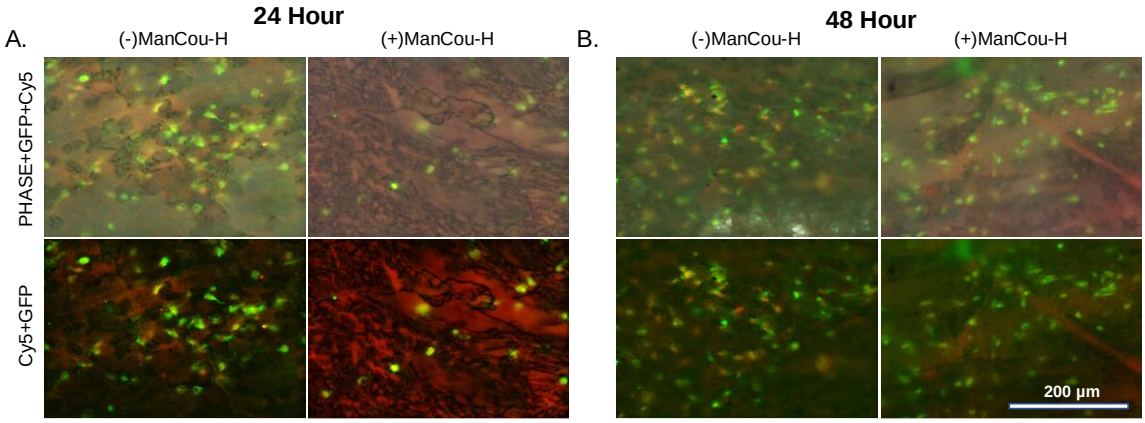

Figure 51 MDA-MB-231 cells seeded on aligned scaffolds and immuno-stained for cytokeratin-18, with the nucleus stained red. Imaged in phase, GFP and Cy5 (A) 24 hours with and without 20µM ManCou-H media (B) 48 hours with and without 20µM ManCou-H media. Images captured at 20x magnification.

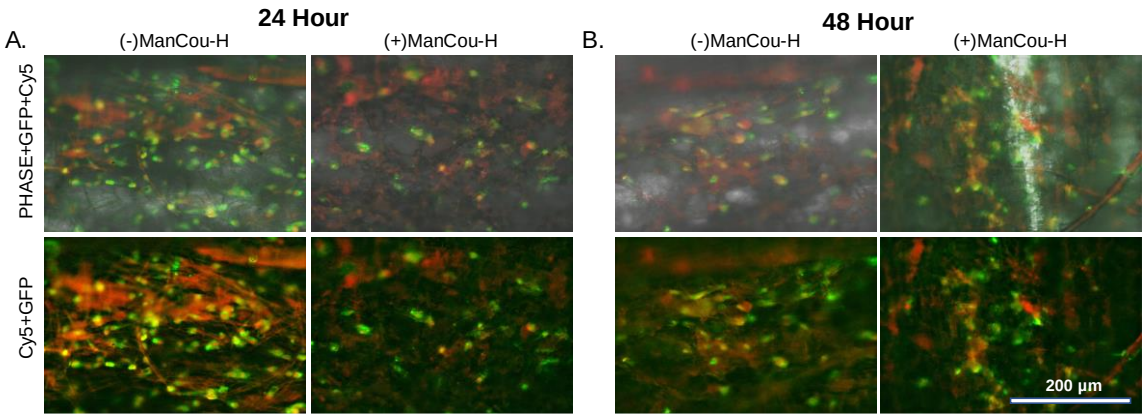

Figure 52 MDA-MB-231 cells seeded on honeycomb scaffolds and immuno-stained for cytokeratin-18, with the nucleus stained red. Imaged in phase and Cy5 (A) 24 hours with and without 20µM ManCou-H media (B) 48 hours with and without 20µM ManCou-H media. Images captured at 20x magnification.

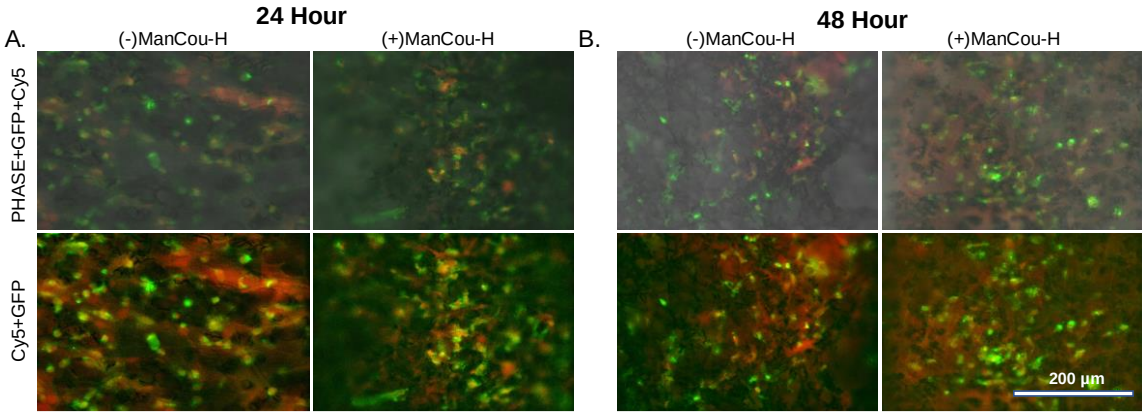

Figure 53 MDA-MB-231 cells seeded on mesh scaffolds and immuno-stained for cytokeratin-18, with the nucleus stained red. Imaged in phase, GFP and Cy5 (A) 24 hours with and without 20µM ManCou-H media (B) 48 hours with and without 20µM ManCou-H media. Images captured at 20x magnification.

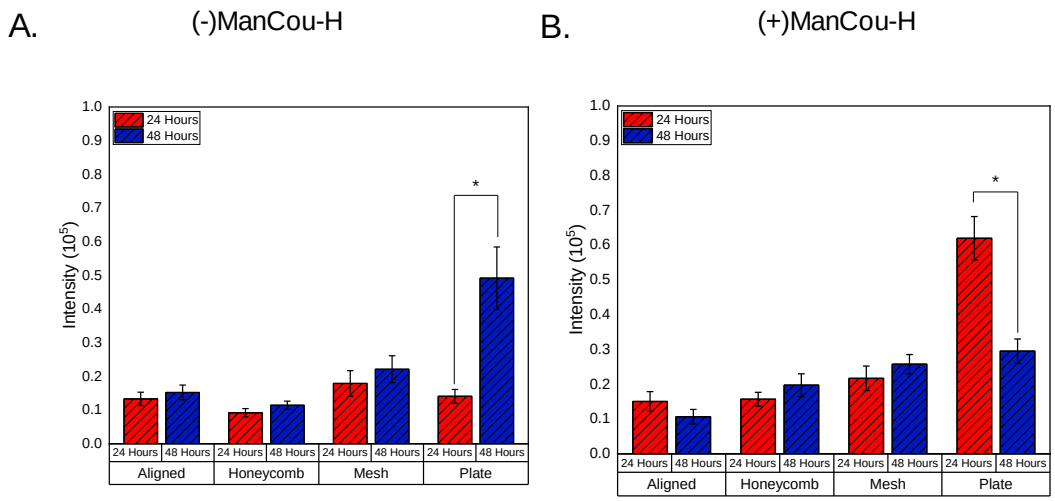

Figure 54 Intensity of MDA-MB-231 cells stained against cytokeratin-18 antibody on aligned, honeycomb, mesh scaffolds as well as the 2D culture plate after 24h and 48h in (A) regular culture media, and (B) in ManCou-H containing media. Cell seeding density was maintained across all groups. Error bars represent the standard error of mean.

In Figure 40 and Figure 50 cytokeratin-18 intensity in 184B5 and MDA-MB-231 cells seeded on 2D culture plate is faint. There is an increase in intensity in cytokeratin-18 in both 184B5 and MDA-MB-231 cell types that were seeded on scaffolds when compared to the 2D culture plates (Figures 41-43, 51-53). MCF7 cells appear to have high cytokeratin-18 intensity in both the 2D culture plate as well as the scaffolds (Figures 45-48). Figures 43 and 48 do not have images for 184B5 cells and MCF7 cells on mesh scaffolds at 24h without probe, and due to the recent campus shutdown, images were not able to be taken and therefore they are not included in the figure.

Figure 44 shows similar cytokeratin-18 intensity in 184B5 cells in the non-treated group on the 2D culture plate as well as the honeycomb scaffolds. There is an increase in cytokeratin-18 intensity in the aligned and mesh scaffold types in the non-treated groups. Cytokeratin-18 intensity in the 184B5 cells treated with ManCou-H show an increase in intensity across all scaffold types after 24h and 48h, while remaining similar on the 2D culture plate after 24h and 48h. Figure 49 shows a trend in MCF7 cells in that in honeycomb scaffolds, mesh scaffolds, and 2D culture plates there is an increase in cytokeratin-18 intensity in both treated and non-treated groups after 24h and 48h. What's most notable is the apparent switch in intensity on the aligned scaffolds after 24h and 48h. In the non-treated group, cytokeratin-18 expression decreases after 24h, but in the treated group, it increases after 24hr. Finally, Figure 54 shows the cytokeratin-18 intensity for MDA-MB-231. Cytokeratin-18 intensity varies differently between each scaffold type but remains consistent on the 2D culture plate. On the aligned scaffolds when treated with ManCou-H, cytokeratin-18 levels decrease after 24h but are shown to increase on the aligned scaffolds

when not treated with ManCou-H. In both the treated and non-treated groups on the honeycomb scaffolds there is an increase in cytokeratin-18 intensity after 24h.

3.4 Flow Cytometer Analysis of ManCou-H uptake in MCF7

In order to evaluate difference in uptake of the ManCou-H probe between cells on scaffolds and cells on cultures, the uptake of the ManCou-H probe was evaluated using the MCF7 cells. Figure 55 shows the MCF7 incubated in cell tracker red that have been either treated with 20μM ManCou-H probe containing media or just grown in standard culture media. Figure 55A shows MCF7 cells gated for cell tracker red, and below shows the absence of the ManCou-H probe. Figure 55B shows the MCF7 cells gated for the cell tracker red, and below shows the presence of the ManCou-H probe in a portion of the population.

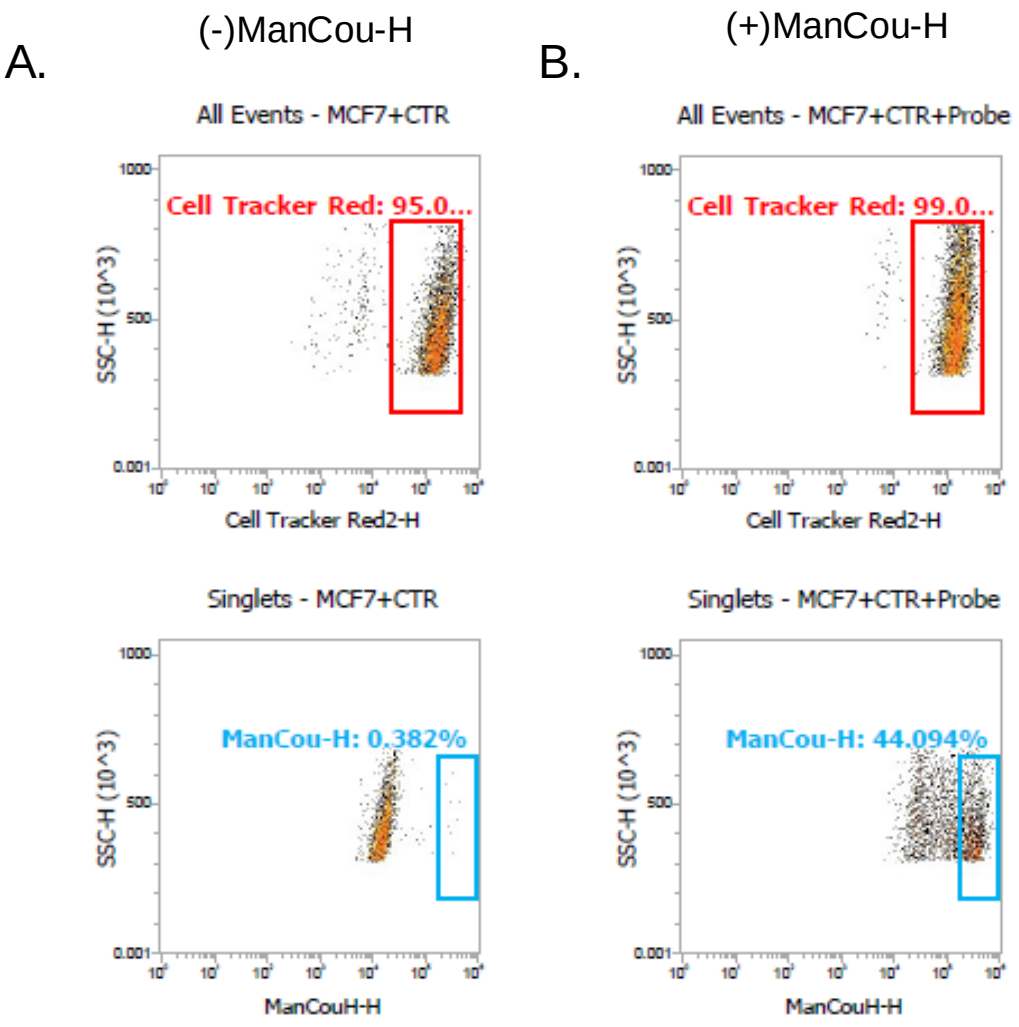

Figure 55 Flow cytometry analysis of MCF7 cells in cell tracker red after a 60 minute incubation (A) without ManCou-H probe containing media and (B) with ManCou-H probe containing media.

This is preliminary data as further experiments were planned to analyze ManCou-H uptake across all three cell lines as well as seeded onto 2D culture plates and the three different scaffold types. Due to the university shutdown, these experiments were not able to be carried out, however the data that we did obtain is shown here.

4 Discussion

The extracellular matrix has long been established as providing cells, tissues and organs with structural and mechanical support and aids in cell differentiation, proliferation, gene expression, and cell motility. Among the different ways that the ECM can remodel, it also possesses the ability to harden and become more stiff which can initiate a number of neoplastic diseases such as breast cancer, and even aid in their progression [43]. Traditional 2D culture methods have been widely accepted in studying cell behavior *ex vivo* and has been used as a tool in providing knowledge as to how cells behave when subjected to various external stimuli. There is a shift however from using 2D cell culture methods to 3D structures in order to mimic the biochemical and biomechanical microenvironments inside the human body. 3D scaffolds have been used as tools to help understand how the ECM affects cell behavior [44-46]. Biopolymers such as hyaluronic acid, gelatin and collagen have been successfully derived from animal tissues however, prefabricated scaffolds provide a different level of customizability in the composition, topography and mechanical properties [28].

Here we used electrospun PCL scaffolds in order to investigate its potential in providing a new culture platform that better mimics the ECM structure. What is notable about the scaffolds is that they are not pre-treated with any adhesion promoter as 2D culture plates usually are. This means that both the breast cancer cells as well as the breast normal cells were able to adhere to the bare scaffolds without the aid of adhesion molecules. We observed differing cell behavior between single cell lines as well as cells in coculture in the way they aggregate and form colonies. On 2D culture plates, cells seem to form distinct colonies and proliferate off those colonies. On scaffolds, cells appear to migrate more so in single cells, embedding themselves withing the nanostructures of the scaffolds. In cocultures, cells on 2D culture plates form intertwined colonies, the cocultures on scaffolds show that cells of differing types tend to segregate more than they cluster together. This could be due to the dimensionality provided by the scaffolds and the contact guidance of each topography which allows for cells to travel in more directions than just one.

Previous studies have shown that breast cancer cell lines as well as breast normal cells that are cultured in 2D vary in gene expression and cell behavior compared to cells cultured on 3D gels of laminin-rich basement membrane [4]. As mentioned previously, breast cancer cells such as MCF7 and MDA-MB-231 have been shown to overexpress GLUT5, which normal breast epithelial cells do not [39]. However, other studies claim that breast cancer cells do not overexpress GLUT5 [47]. For this reason, we sought to evaluate the levels of GLUT5 expression in 184B5, MCF7 and MDA-MB-231 using the 2D and 3D culture platforms. We also subjected the cell cultures to not only standard cell culture media, but also culture media containing the fluorescent fructose mimic, ManCou-H.

In both the treated and non-treated groups, GLUT5 expression is similar after 24h and 48h among all three cell lines. However, the levels of GLUT5 expression vary not only after 24h and 48h but also varies among scaffold types in the treated and non-treated groups in all three cell lines. This variation indicates that over time cells will express GLUT5 at

different levels in a 3D environment as opposed to a 2D environment where the GLUT5 expression remains similar.

Another biomarker we evaluated was cytokeratin-18. Cytokeratin-18 is specific to epithelial cells and has been shown to be involved in cell motility as well as cancer progression [48]. Specifically, the downregulation of cytokeratin-18 has been reported to promote the progression of breast cancer and is associated with lowered life expectancy [49]. What we've seen were similar expression profiles between 184B5 and MDA-MB-231. This result was expected in the highly metastatic breast cancer cells, however unexpected in the normal epithelial breast cells, 184B5. As of current, there is no reported data on cytokeratin-18 expression in 184B5. In the MCF7 cells cultured on the 2D culture plates show similar increased amounts of cytokeratin-18 after 24h and 48h. On the scaffolds, the cytokeratin-18 expression in MCF7 varies greatly, most notable is the difference observed in the aligned scaffolds of the treated and non-treated groups. Aligned scaffolds have been previously reported to give MCF7 cells contact guidance and explains why cytokeratin-18 expression decreased in non-treated groups after 24h indicating cell movement. It appears adding ManCou-H to MCF7 cells on aligned scaffolds causes a reverse effect where cytokeratin-18 expression increases after 24h.

The present investigation sought to evaluate 3D PCL scaffolds as a cell culture platform that could mimic the ECM and highlight differences in culturing cells in 3D versus the traditional 2D culture plate. These observations support that cellular behavior and gene expression is different among the two platforms.

The flow cytometry analysis of ManCou-H uptake in the MCF7 cells shows promise to allow for further studies to analyze probe uptake among the three different cells lines seeded onto 2D culture plates as well as the 3D scaffolds. This information could provide more insight as to metabolic behavior of cells that are cultured in 2D culture plates versus 3D scaffolds.

5 Conclusion

The present investigation demonstrated that breast normal as well as breast cancer cell lines behave differently when cultured on conventional 2D culture plates versus 3D electrospun PCL scaffolds. Cells cultured on scaffolds not only behave differently in colony formation and in cell morphology, but they also exhibit varying levels of GLUT5 and cytokeratin-18 than cell cultured on culture plates. This indicates that cells will exhibit different cellular behavior and gene expression depending on the environment they are cultured in. Therefore, type of culture environment should be taken into consideration in experimental planning. Synthetic scaffolds are of interest to researchers and engineers due to its simplicity in production, batch to batch consistency and reliability, low cost and its ability to better mimic the biological environment of the ECM than the traditional 2D culture plate. Ideally, scaffolds can be used as another tool for scientists to plan experiments using user defined 3D platforms. Even though 3D scaffolds bring science and engineering closer to mimicking in vivo physiological conditions than 2D culture plates, further studies are needed to replicate these conditions more accurately.

6 Reference List

1. Cavo, M., et al., *Microenvironment complexity and matrix stiffness regulate breast cancer cell activity in a 3D in vitro model.* Scientific reports, 2016. **6**: p. 35367.
2. Hynes, R.O., *The extracellular matrix: not just pretty fibrils.* Science, 2009. **326**(5957): p. 1216-1219.
3. Yue, B., *Biology of the extracellular matrix: an overview.* Journal of glaucoma, 2014: p. S20.
4. Bissell, M.J., et al., *The organizing principle: microenvironmental influences in the normal and malignant breast.* Differentiation: REVIEW, 2002. **70**(9-10): p. 537-546.
5. Ulrich, T.A., E.M. de Juan Pardo, and S. Kumar, *The mechanical rigidity of the extracellular matrix regulates the structure, motility, and proliferation of glioma cells.* Cancer research, 2009. **69**(10): p. 4167-4174.
6. Jena, M.K. and J. Janjanam, *Role of extracellular matrix in breast cancer development: a brief update.* F1000Research, 2018. **7**.
7. Wang, Y. and B.P. Zhou, *Epithelial-mesenchymal transition in breast cancer progression and metastasis.* Chinese journal of cancer, 2011. **30**(9): p. 603.
8. Wu, Y., M. Sarkissyan, and J.V. Vadgama, *Epithelial-mesenchymal transition and breast cancer.* Journal of clinical medicine, 2016. **5**(2): p. 13.
9. Bill, R. and G. Christofori, *The relevance of EMT in breast cancer metastasis: Correlation or causality?* FEBS letters, 2015. **589**(14): p. 1577-1587.
10. Fuchs, E. and K. Weber, *Intermediate filaments: structure, dynamics, function and disease.* Annual review of biochemistry, 1994. **63**(1): p. 345-382.
11. Coulombe, P.A. and P. Wong, *Cytoplasmic intermediate filaments revealed as dynamic and multipurpose scaffolds.* Nature cell biology, 2004. **6**(8): p. 699-706.
12. Weng, Y.-R., Y. Cui, and J.-Y. Fang, *Biological functions of cytokeratin 18 in cancer.* Molecular Cancer Research, 2012. **10**(4): p. 485-493.
13. Schaller, G., et al., *Elevated keratin 18 protein expression indicates a favorable prognosis in patients with breast cancer.* Clinical Cancer Research, 1996. **2**(11): p. 1879-1885.
14. Infanger, D.W., M.E. Lynch, and C. Fischbach, *Engineered culture models for studies of tumor-microenvironment interactions.* Annual review of biomedical engineering, 2013. **15**: p. 29-53.
15. Mak, I.W., N. Evaniew, and M. Ghert, *Lost in translation: animal models and clinical trials in cancer treatment.* American journal of translational research, 2014. **6**(2): p. 114.
16. Kelm, J.M. and M. Fussenegger, *Microscale tissue engineering using gravity-enforced cell assembly.* Trends in biotechnology, 2004. **22**(4): p. 195-202.
17. Duval, K., et al., *Modeling physiological events in 2D vs. 3D cell culture.* Physiology, 2017. **32**(4): p. 266-277.
18. Mehta, G., et al., *Opportunities and challenges for use of tumor spheroids as models to test drug delivery and efficacy.* Journal of controlled release, 2012. **164**(2): p. 192-204.
19. Tibbitt, M.W. and K.S. Anseth, *Hydrogels as extracellular matrix mimics for 3D cell culture.* Biotechnology and bioengineering, 2009. **103**(4): p. 655-663.
20. Lee, S.-H., J.J. Moon, and J.L. West, *Three-dimensional micropatterning of bioactive hydrogels via two-photon laser scanning photolithography for guided 3D cell migration.* Biomaterials, 2008. **29**(20): p. 2962-2968.

21. Salinas, C.N. and K.S. Anseth, *The enhancement of chondrogenic differentiation of human mesenchymal stem cells by enzymatically regulated RGD functionalities.* Biomaterials, 2008. **29**(15): p. 2370-2377.
22. Mann, B.K. and J.L. West, *Cell adhesion peptides alter smooth muscle cell adhesion, proliferation, migration, and matrix protein synthesis on modified surfaces and in polymer scaffolds.* Journal of biomedical materials research, 2002. **60**(1): p. 86-93.
23. West, J.L. and J.A. Hubbell, *Polymeric biomaterials with degradation sites for proteases involved in cell migration.* Macromolecules, 1999. **32**(1): p. 241-244.
24. Han, L.-H., et al., *Dynamic tissue engineering scaffolds with stimuli-responsive macroporosity formation.* Biomaterials, 2013. **34**(17): p. 4251-4258.
25. Lee, K. and J.A. Hubbell, *Tissue, cell and engineering.* Current opinion in biotechnology, 2013. **5**(24): p. 827-829.
26. Vatankhah, E., et al., *Artificial neural network for modeling the elastic modulus of electrospun polycaprolactone/gelatin scaffolds.* Acta biomaterialia, 2014. **10**(2): p. 709-721.
27. Subia, B., J. Kundu, and S. Kundu, *Biomaterial scaffold fabrication techniques for potential tissue engineering applications.* Tissue engineering, 2010. **141**.
28. Hanumantharao, S.N., et al., *Electrospun acellular scaffolds for mimicking the natural anisotropy of the extracellular matrix.* RSC Advances, 2019. **9**(69): p. 40190-40195.
29. Naeimirad, M., et al., *Recent advances in core/shell bicomponent fibers and nanofibers: A review.* Journal of Applied Polymer Science, 2018. **135**(21): p. 46265.
30. Agnihotri, S. and G. Zadeh, *Metabolic reprogramming in glioblastoma: the influence of cancer metabolism on epigenetics and unanswered questions.* Neuro-Oncology, 2015. **18**(2): p. 160-172.
31. Xu, X.D., et al., *Warburg effect or reverse Warburg effect? A review of cancer metabolism.* Oncology research and treatment, 2015. **38**(3): p. 117-122.
32. Scharping, N.E. and G.M. Delgoffe, *Tumor microenvironment metabolism: a new checkpoint for anti-tumor immunity.* Vaccines, 2016. **4**(4): p. 46.
33. Szablewski, L., *Expression of glucose transporters in cancers.* Biochimica et Biophysica Acta (BBA)-Reviews on Cancer, 2013. **1835**(2): p. 164-169.
34. Schwartzenberg-Bar-Yoseph, F., M. Armoni, and E. Karnieli, *The tumor suppressor p53 down-regulates glucose transporters GLUT1 and GLUT4 gene expression.* Cancer research, 2004. **64**(7): p. 2627-2633.
35. Godoy, A., et al., *Differential subcellular distribution of glucose transporters GLUT1–6 and GLUT9 in human cancer: ultrastructural localization of GLUT1 and GLUT5 in breast tumor tissues.* Journal of cellular physiology, 2006. **207**(3): p. 614-627.
36. Charrez, B., L. Qiao, and L. Hebbard, *The role of fructose in metabolism and cancer.* Hormone molecular biology and clinical investigation, 2015. **22**(2): p. 79-89.
37. Liu, H. and A.P. Heaney, *Refined fructose and cancer.* Expert opinion on therapeutic targets, 2011. **15**(9): p. 1049-1059.
38. Port, A.M., M.R. Ruth, and N.W. Istfan, *Fructose consumption and cancer: is there a connection?* Current Opinion in Endocrinology, Diabetes and Obesity, 2012. **19**(5): p. 367-374.
39. Zamora-León, S.P., et al., *Expression of the fructose transporter GLUT5 in human breast cancer.* Proceedings of the National Academy of Sciences, 1996. **93**(5): p. 1847-1852.

40. Levi, J., et al., *Fluorescent fructose derivatives for imaging breast cancer cells.* Bioconjugate chemistry, 2007. **18**(3): p. 628-634.
41. Tanasova, M., et al., *Fluorescent THF-based fructose analogue exhibits fructose-dependent uptake.* ChemBioChem, 2013. **14**(10): p. 1263-1270.
42. Begoyan, V.V., et al., *Multicolor GLUT5-permeable fluorescent probes for fructose transport analysis.* Chemical communications, 2018. **54**(31): p. 3855-3858.
43. Sonbol, H.S., *Extracellular matrix remodeling in human disease.* Journal of microscopy and ultrastructure, 2018. **6**(3): p. 123.
44. Cukierman, E., et al., *Taking Cell-Matrix Adhesions to the Third Dimension.* Science, 2001. **294**(5547): p. 1708-1712.
45. Khalil, S. and W. Sun, *Bioprinting endothelial cells with alginate for 3D tissue constructs.* Journal of biomechanical engineering, 2009. **131**(11).
46. Place, E.S., N.D. Evans, and M.M. Stevens, *Complexity in biomaterials for tissue engineering.* Nature materials, 2009. **8**(6): p. 457-470.
47. Gowrishankar, G., et al., *GLUT 5 is not over-expressed in breast cancer cells and patient breast cancer tissues.* PloS one, 2011. **6**(11).
48. Wang, H., et al., *Effect of chymotrypsin C and related proteins on pancreatic cancer cell migration.* Acta Biochim Biophys Sin, 2011. **43**(5): p. 362-371.
49. Woelfle, U., et al., *Down-regulated expression of cytokeratin 18 promotes progression of human breast cancer.* Clinical cancer research, 2004. **10**(8): p. 2670-2674.